Cooling curves for neutron stars with hadronic matter and quark matter

Shaoyu Yin[1*], J.J.R.M. van Heugten[1], Jeroen Diederix[1], Maarten Kater[1], Jacco Vink[2], and H.T.C. Stoof[1]

1. Institute for Theoretical Physics, Utrecht University,
Leuvenlaan 4, 3584 CE Utrecht, The Netherlands
2. Astronomical Institute, Utrecht University, P.O. Box 80000, 3508 TA Utrecht, The Netherlands

The thermal evolution of isothermal neutron stars is studied with matter both in the hadronic phase as well as in the mixed phase of hadronic matter and strange quark matter. In our models, the dominant early-stage cooling process is neutrino emission via the direct Urca process. As a consequence, the cooling curves fall too fast compared to observations. However, when superfluidity is included, the cooling of the neutron stars is significantly slowed down. Furthermore, we find that the cooling curves are not very sensitive to the precise details of the mixing between the hadronic phase and the quark phase and also of the pairing that leads to superfluidity.

I. INTRODUCTION

Neutron stars are natural laboratories for physics under extreme conditions with their extremely high densities, powerful energy emission, large magnetic fields, and millisecond rotation periods. At the densities near the surface of such a star, atoms break apart into nuclei and electrons. At higher densities, the electrons neutralize with the protons in the nuclei to form neutrons. These stars thus consist of a large fraction of neutrons and are supported from gravitational collapse by the neutron degeneracy pressure, from which the neutron star derives its name.

However, at high densities the existence of more exotic particles is expected. These particles are generated by processes which produce strangeness, such as

$$n + n \rightarrow n + \Lambda^0 + K^0, \tag{1}$$

where n is the neutron, Λ^0 the Lambda hyperon, and K^0 the strange meson. The strange meson can decay via various weak processes and the final products, usually photons and neutrinos, leak out of the star. Therefore, the reverse process is reduced and some net amount of strangeness survives in the dense core of the star [1]. It is generally believed that these strangeness carrying particles, called hyperons, can exist in the center of neutron stars. They coexist with the nucleons as well as the leptons e^- and μ^-. The interactions between them are dominated by the complicated nuclear force whose carriers are the mesons. We refer to such a system as the hadronic phase of matter. The system with only nucleons and leptons, i.e., without hyperons, is referred to as the nuclear phase of matter.

At even higher densities, as a consequence of asymptotic freedom, quarks become deconfined from the hadrons. Therefore, strange quark matter, which consists of u, d and s quarks, may also exist in the neutron
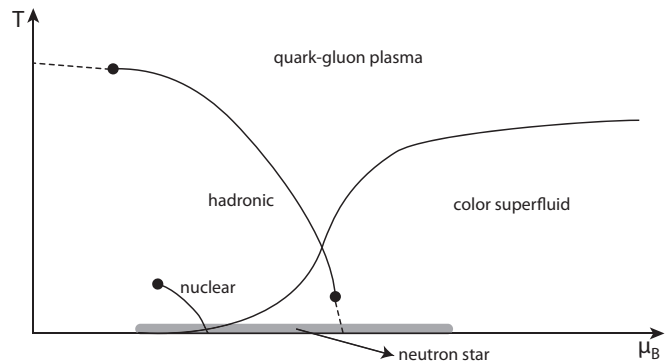

FIG. 1: The schematic QCD phase diagram as a function of temperature T and baryon chemical potential μ_B. The solid lines denote first- and second-order phase transitions, whereas the dashed lines denote smooth crossovers. According to the typical temperature of a proto-neutron star of $T \sim 10^{10}$ K ~ 1 MeV, the state of matter in the neutron star should be close to the bottom line, as indicated by the grey thick line.

star core. There may also be a phase-separated mixture of strange quark matter and hadronic matter in a certain range of densities [2], which we call the mixed phase. At present, there is still a lot unknown about the deconfinement phase transition of quarks. The contemporary knowledge on matter at high densities and temperatures is shown by the schematic QCD phase diagram in Fig. 1. Since the baryon chemical potential μ_B is a monotonously increasing function from the surface to the center of the neutron star, the μ_B axis can be mapped to the stellar radius and the different phases in the neutron star are explicitly indicated.

Because of the limited knowledge on the state of matter at high densities and the complexity of the interactions between the particles, many effective models for matter inside neutron stars have been constructed. In general, these models supply an equation of state, which determines the particle composition of the neutron star. The observation of neutron stars, in turn, constrain these models. For example, if an equation of state is too soft it is incapable of supporting a very large stellar mass,

such that some models become disfavored whenever the data on the heaviest neutron star is updated. The stellar mass is not the only constraint on the models. The cooling of neutron stars can be studied from their luminosity as a function of time. A proto-neutron star is born with a typical temperature larger than 10^{10} K, after which it mainly loses its energy by two processes, namely by neutrino emission everywhere inside the star and by photon radiation at the surface. In the early stages of the thermal evolution of the star, neutrino emission is the dominant cooling effect after which photon radiation ultimately takes over [3]. Since neutrino emission occurs everywhere in the neutron star, it provides a probe for studying the state of matter inside the star.

The most efficient neutrino-emission process is called the direct Urca (DUrca) process

$$n \rightarrow p + e^- + \bar{\nu}_e, \quad p + e^- \rightarrow n + \nu_e. \qquad (2)$$

This process is only possible if the proton fraction is more than a certain threshold in order for it to satisfy energy and momentum conservation [4]. Historically, the proton abundance in neutron stars was underestimated. In that scenario, it is reasonable to take into account also the modified Urca (MUrca) process, where a bystander helps the momentum conservation, for example

$$n + n \rightarrow p + n + e^- + \bar{\nu}_e, \, p + n + e^- \rightarrow n + n + \nu_e,$$
$$n + p \rightarrow p + p + e^- + \bar{\nu}_e, \, p + p + e^- \rightarrow n + p + \nu_e. \quad (3)$$

Some other processes can have a neutrino emissivity which is smaller or comparable to the modified Urca process, such as neutrino bremsstrahlung and plasmon decay [3]. However, all of them are negligible whenever the direct Urca channel is open. In the hadronic phase, the direct Urca processes are quite rich and can be summarized as

$$b_1 \rightarrow b_2 + l^- + \bar{\nu}_l, \quad b_2 + l^- \rightarrow b_1 + \nu_l, \qquad (4)$$

where b_1 and b_2 denote two different baryons and l^- represents one of the leptons, e^- or μ^-.

For strange quark matter, the direct Urca processes are

$$d \rightarrow u + l^- + \bar{\nu}_l, \quad u + l^- \rightarrow d + \nu_l,$$
$$s \rightarrow u + l^- + \bar{\nu}_l, \quad u + l^- \rightarrow s + \nu_l, \qquad (5)$$

which are simply the direct Urca processes of the baryons at the quark level. Inside the neutron star, there is no threshold for the direct Urca process in quark matter, since the Fermi momenta of the two quarks and lepton can always satisfy momentum conservation. As mentioned, the neutrino emissivity depends strongly on the type of matter contributing to the process, such that the thermal evolution of a star directly probes its composition. The main goal of this paper is to study the cooling of neutron stars with different types of equations of state and try to constrain them by comparing with observational data.

A large amount of research on the cooling process of neutron stars has been carried out in the last several decades, with a strong focus on the nuclear phase of matter. To the best of our knowledge, a unifying model covering the low-density nuclear phase to the deconfined quark phase, consistent with the QCD phase diagram, has been less thoroughly explored. The strange quark star composed of strange matter, either with or without the nuclear crust, has been considered in some papers [5, 6]. However, the cooling behavior of neutron stars containing also all hyperons and possibly also a mixed phase of strange quark matter and hadronic matter, has not been extensively studied. Two possible reasons for this can be given. First, the hadronic and mixed equations of state are rather soft and are continuously being challenged by new data on heavy neutron stars, such as PSR J1903+0327 which has $M = 1.67 \pm 0.01$ M$_\odot$ [7] and PSR J1614−2230 which even has $M = 1.97 \pm 0.04$ M$_\odot$ [8]. Second, the existence of a mixed phase is being questioned in view of screening and surface effects [9]. With respect to the first concern, we note that most of the observed neutron star masses still lie below the maximum mass a hadronic or mixed equation of state can allow for. According to Ref. [10], most nearby young neutron stars [11] have masses no bigger than 1.4 M$_\odot$ [12]. Therefore, at least for the study of the thermal evolution of these stars, the hadronic or mixed phase can still be of great importance. In fact, because of the uncertainties in the interaction between particles at extremely high density, it is hard to exactly determine the equation of state at high density. Although the equations of state used in this paper cannot support neutron stars as massive as those reported above, we can still use them for a discussion on medium-mass neutron stars with more complicated compositions. As for the stability of the mixed phase, the arguments are still indecisive. For example, many details of the surface tension, which strongly influences the stability calculation, are still uncertain. Although it is expected that screening and surface effects diminish the mixed-phase regime, it is far from certain that its existence can be excluded [13]. The mixed phase can in particular have significant effects on the cooling behavior, especially for the heat transport inside the star. However, we show below that its effect will be less important after the star has become isothermal, when the thermal evolution is determined by the heat capacity and neutrino emissivity integrated over the whole volume, and the inner thermal conductivity no longer plays a role.

The temperature of a neutron star is generally much smaller than the typical Fermi energy as a consequence of the very high densities in the star. Therefore, superfluidity may play an important role. According to BCS theory, fermions can form Cooper pairs at low temperatures via an attractive interaction and thereby lower the energy of the system. The resulting pairs, which obey Bose statistics, can form a Bose-Einstein condensate and the system becomes superfluid. Pair formation changes the single-particle dispersion around the Fermi surface

and consequently the heat capacity and neutrino emissivity will be influenced. We find that, without superfluidity, the cooling of neutron stars is too fast compared with observations. However, by including the effects of superfluidity we obtain a more realistic cooling behavior.

The quark phase is usually referred to as an exotic phase of extremely dense matter, in contrast to the nuclear phase or the hadronic phase. Other exotic phases have also been proposed, among which the pion and kaon condensates have attracted much attention [14, 15]. However, the existence of such phases inside the neutron star is still an open question. On the one hand, with such condensates, the equation of state is further softened and thus the corresponding maximum star mass is reduced [16], which makes such phases less favored when compared to the observational data of massive stars, as mentioned above. On the other hand, for the cooling process, it was reported that a meson condensate can increase the neutrino emissivity over the typical modified Urca emissivity by several orders of magnitude [3], but it is still much less efficient than the direct Urca process. Since in our calculation the direct Urca process is always present, such enhancement from the meson condensate has a negligible effect. Besides, the kaon condensation may even reduce the pressure and cause the star to collapse into a black hole [15]. Therefore, considering all the above arguments, we do not include such meson condensates in this paper.

The paper is organized as follows, we first introduce in Sec. II our theoretical framework which includes the relativistic stellar structure, the unified mean-field model describing the state of matter inside the star, and the thermal evolution equations. In Sec. III, we then present the numerical results for the cooling curves of neutron stars with the nuclear, hadronic, and mixed equations of state. Due to the efficiency of the direct Urca process the cooling is seen to be too fast compared to observations. Therefore superfluidity is included in Sec. IV and, as a consequence, the cooling is slowed down and we find a much better agreement with observations.

II. THEORETICAL FRAMEWORK

At the high densities of importance to neutron stars the neutrons, protons, and electrons can be considered to be highly degenerate. In particular, the typical Fermi temperature of the nucleons is about 10^{12} K while the temperature of a proto-neutron star is only 10^{10} K. This provides a great theoretical advantage since it makes it possible to decouple the calculation of the stellar structure, the nuclear model, and the thermal evolution of the star. In other words, the thermal evolution of the star depends on the stellar structure, which in turn is constructed from the nuclear model. The nuclear model will be solved in the zero-temperature limit to give the equation of state. The stellar structure is then obtained from Einstein's equations using this equation of state.

Although many neutron stars have fast rotation rates and strong magnetic fields, due to the complexity and richness of these phenomenon they are beyond our present discussion. In fact, the effect of rotation should be quite small for most of the neutron stars except for millisecond pulsars. Therefore, Einstein's equations are solved for static stars without magnetic fields. Furthermore, the star interior is approximated by a perfect fluid, i.e., it is hydrostatic, which is valid as long as the energy transported by heat conduction is negligible compared to the total energy. Subsequently, to discuss the thermal evolution, some properties of the stellar matter, such as the heat capacities, conductivities, and emissivities, can be obtained by considering a perturbation of the Fermi surfaces of the various particles. In the following, we deal with these aspects of our theoretical framework separately.

A. The general relativistic profile of a compact star

The space-time metric for a non-rotating, spherically symmetric star can be written as

$$ds^2 = e^{2\Phi(r)}c^2dt^2 - e^{2\lambda(r)}dr^2 - r^2(d\theta^2 + \sin^2\theta d\phi^2), \quad (6)$$

where $\Phi(r)$ is the metric function related to the gravitational redshift, $\exp[-2\lambda(r)] = 1 - 2Gm(r)/c^2r$ with $m(r) = \int_0^r 4\pi r'^2 \rho(r')dr'/c^2$ the gravitational mass enclosed within the sphere of radius r, G is the gravitational constant, and c is the speed of light. As a consequence of the above metric, Einstein's equations for the case of a non-rotating, hydrostatic, and spherically symmetric star reduce to the Tolman-Oppenheimer-Volkoff (TOV) equations, namely

$$\frac{d\Phi(r)}{dr} = -\frac{1}{\rho(r) + p(r)}\frac{dp(r)}{dr}, \quad (7)$$

$$\frac{dp(r)}{dr} = -\frac{[\rho(r) + p(r)]G[m(r) + 4\pi r^3 p(r)/c^2]}{c^2 r^2 \left[1 - \frac{2Gm(r)}{c^2 r}\right]}, \quad (8)$$

where $p(r)$ and $\rho(r)$ are the pressure and energy density at radius r, respectively. Given an equation of state $p(\rho)$, the TOV equations can be numerically integrated to provide the structure of the star. The integration starts at $r = 0$ with a given pressure $p(0) = p_c$ until $p(R) = 0$ is reached, which defines the radius R of the star. Outside the star, $r > R$, the metric reduces to the Schwarzschild form, $\exp[2\Phi(r)] = \exp[-2\lambda(r)] = 1 - 2GM/c^2r$, where $M = m(R)$ is the total gravitational mass of the star. Note that with the help of a local Lorenz transformation we are always able to apply a locally inertial coordinate system [17] such that the calculation of the equation of state is performed in a homogeneously flat background. Nevertheless, the TOV equations take into account the effects of general relativity on the structure of the star. However, to calculate this structure we need to supply a realistic equation of state for the matter inside a neutron star.

B. Effective model for matter in neutron stars

To obtain an equation of state for stellar matter, we apply an effective nuclear model which includes all relevant kinds of baryons. The interactions between the baryons are mediated by three types of effective meson fields, namely the scalar meson σ, the vector meson ω_μ and the isovector meson $\vec{\rho}_\mu$. The scalar field is coupled to the derivatives of the baryon field as shown in the following Lagrangian density [2]:

$$
\begin{aligned}
\mathcal{L} = \sum_b &\left[\left(1 + \frac{g_{\sigma b}\sigma}{m_b c^2}\right) \bar{\psi}_b \left(i\hbar c\gamma_\mu \partial^\mu - g_{\omega b}\gamma_\mu \omega^\mu \right.\right.\\
&\left.\left. - \frac{1}{2}g_{\rho b}\gamma_\mu \vec{\tau}\cdot\vec{\rho}^\mu \right)\psi_b - m_b c^2 \bar{\psi}_b \psi_b \right] + \frac{\hbar\partial_\mu\sigma\partial^\mu\sigma}{2c^3} \\
&- \frac{m_\sigma^2 \sigma^2}{2\hbar c} - \frac{\hbar\omega_{\mu\nu}\omega^{\mu\nu}}{4c^3} + \frac{m_\omega^2 \omega_\mu \omega^\mu}{2\hbar c} - \frac{\hbar\vec{\rho}_{\mu\nu}\vec{\rho}^{\mu\nu}}{4c^3} \\
&+ \frac{m_\rho^2 \vec{\rho}_\mu \vec{\rho}^\mu}{2\hbar c} + \sum_l \bar{\psi}_l(i\hbar c\gamma_\mu \partial^\mu - m_l c^2)\psi_l,
\end{aligned}
\tag{9}
$$

where $c\partial_0 = \partial/\partial t$, the summation over b and l is over all contributing baryon fields ψ_b and lepton fields ψ_l, and in the meson kinetic terms $\omega_{\mu\nu} \equiv \partial_\mu\omega_\nu - \partial_\nu\omega_\mu$ and $\vec{\rho}_{\mu\nu} \equiv \partial_\mu\vec{\rho}_\nu - \partial_\nu\vec{\rho}_\mu$ are the antisymmetric field strengths. The derivative coupling of the σ field was first introduced by Zimanyi and Moszkowski [18] to remove the problem of a too small or even negative reduced baryon mass (commonly referred to as the effective mass, however, this name is used in this paper only for the effective fermion mass on the Fermi surface) at high density in the standard Walecka model [19].

This model can be solved within the mean-field approximation. In this approximation all the meson fields are replaced by their ground-state expectation values, which are constants in space-time and their spatial components are zero because the system is assumed to be homogeneous and isotropic. Also the charged components of the isospin vector ρ^+ and ρ^-, whose sources are the off-diagonal currents of the baryon fields, are zero. Therefore, only the three constant fields σ, ω^0 and ρ_3^0 survive in the Euler-Lagrange equations. In the following, we simply denote the last two as ω and ρ. Furthermore, the constant scalar field σ can be absorbed into the baryon field and the reduced mass by a rescaling, namely $\Psi_b = \sqrt{1 + \frac{g_{\sigma b}\sigma}{m_b c^2}}\psi_b$ and $\tilde{m}_b(\sigma) = m_b/(1 + \frac{g_{\sigma b}\sigma}{m_b c^2})$. Notice that $\tilde{m}_b$ is positive definite and only approaches zero as $\sigma \to \infty$.

In the mean-field approximation the Lagrangian gives rise to the following field equations:

$$
\left[i\hbar c\gamma^\mu \partial_\mu - g_{\omega b}\gamma_0\omega - \frac{1}{2}g_{\rho b}\gamma_0\tau_3\rho - \tilde{m}_b c^2\right]\Psi_b = 0, \tag{10}
$$

$$
\sum_b \frac{g_{\sigma b}\langle\bar{\Psi}_b\Psi_b\rangle}{\left(1 + \frac{g_{\sigma b}\sigma}{m_b c^2}\right)^2} - \frac{m_\sigma^2 \sigma}{\hbar c} = 0, \tag{11}
$$

$$
\sum_b g_{\omega b}\langle\Psi_b^\dagger\Psi_b\rangle - \frac{m_\omega^2 \omega}{\hbar c} = 0, \tag{12}
$$

$$
\sum_b g_{\rho b}\frac{1}{2}\langle\Psi_b^\dagger\tau_3\Psi_b\rangle - \frac{m_\rho^2 \rho}{\hbar c} = 0, \tag{13}
$$

where $\tau_3/2$ gives the expectation value of the third component of the baryon isospin I_{3b}. The equation of motion of the baryons gives the following energy eigenvalue

$$
\mu_b = \epsilon_b = g_{\omega b}\omega + g_{\rho b}I_{3b}\rho + \sqrt{\hbar^2 c^2 k_b^2 + \tilde{m}_b^2 c^4}. \tag{14}
$$

From the above it is clear that the baryon b only exists when $\mu_b - (g_{\omega b}\omega + g_{\rho b}I_{3b}\rho) > \tilde{m}_b c^2$. The equation of motion of the leptons are simply the free Dirac equations and are not listed here. Thus, the leptons obey the simple relations of a free relativistic Fermi gas:

$$
n_l = f_l\frac{k_l^3}{6\pi^2}, \quad \mu_l = \epsilon_l = \sqrt{\hbar^2 c^2 k_l^2 + m_l^2 c^4}. \tag{15}
$$

For the expectation value of the baryon field we have

$$
\begin{aligned}
\langle\bar{\Psi}_b\Psi_b\rangle &= \frac{f_b}{2\pi^2}\int_0^{k_b} \frac{\tilde{m}_b c^2 k^2 dk}{\sqrt{\hbar^2 c^2 k^2 + \tilde{m}_b^2 c^4}} \\
&= \frac{f_b}{2\pi^2}\frac{\tilde{m}_b c}{2\hbar^3}\left[\hbar k_b\sqrt{\hbar^2 k_b^2 + \tilde{m}_b^2 c^2} \right.\\
&\left. - \tilde{m}_b^2 c^2 \log\left(\frac{\hbar k_b}{\tilde{m}_b c} + \sqrt{1 + \frac{\hbar^2 k_b^2}{\tilde{m}_b^2 c^2}}\right)\right],
\end{aligned}
\tag{16}
$$

and

$$
\langle\Psi_b^\dagger\Psi_b\rangle = n_b = f_b\frac{k_b^3}{6\pi^2}. \tag{17}
$$

In the above equations $f_i = 2J_i + 1$ is the particle degeneracy, while k_i and ϵ_i are the Fermi momentum and Fermi energy, respectively.

Since the whole star is considered to be in equilibrium, the various processes, such as the direct Urca process in Eq. (2) and those involving the hyperons in Eq. (1), impose relations between the chemical potentials of the particles. During these processes the baryon number and electric charge are conserved, which gives rise to the two chemical potentials μ_B and μ_Q for baryon number and electric charge, respectively. The chemical potential for an arbitrary particle with baryon number B_i and charge Q_i, such as a baryon, lepton or quark, can be written as $\mu_i = B_i\mu_B + Q_i\mu_Q$. The particle data for all the fermions used in this paper are listed in Table. I.

TABLE I: Particle Data [20]. Here, M is the particle mass, B is the baryon number, J is the spin, I_3 is the 3-component of the isospin, and Q is the charge.

	particle	M/MeV	B	J	I_3	Q/e
Baryon	p	938.27	1	1/2	1/2	+1
	n	939.57	1	1/2	$-1/2$	0
	Λ^0	1115.7	1	1/2	0	0
	Σ^+	1189.4	1	1/2	1	+1
	Σ^0	1192.6	1	1/2	0	0
	Σ^-	1197.4	1	1/2	-1	-1
	Δ^{++}	1232	1	3/2	$+3/2$	+2
	Δ^+	1232	1	3/2	$+1/2$	+1
	Δ^0	1232	1	3/2	$-1/2$	0
	Δ^-	1232	1	3/2	$-3/2$	-1
	Ξ^0	1315	1	1/2	$+1/2$	0
	Ξ^-	1322	1	1/2	$-1/2$	-1
	Ω^-	1672	1	3/2	0	-1
Lepton	e^-	0.511	0	1/2	0	-1
	μ^-	105.7	0	1/2	0	-1
Quark	u	2.4	1/3	1/2	$+1/2$	$+2/3$
	d	4.9	1/3	1/2	$-1/2$	$-1/3$
	s	105	1/3	1/2	0	$-1/3$

The coupling constants $g_{\sigma b}$, $g_{\omega b}$ and $g_{\rho b}$ for nucleons can be fitted with data of the interactions at densities near the nuclear saturation point. However, for hyperons the values are not known. Here the coupling constants are simply chosen to be equal among the different baryons [2]. Their values are $(g_\sigma/m_\sigma)^2 = 7.487$ fm^2, $(g_\omega/m_\omega)^2 = 2.615$ fm^2 and $(g_\rho/m_\rho)^2 = 4.774$ fm^2. Notice that the ratio of the coupling constant and the corresponding meson mass is enough to solve this model, because we can always rescale the meson fields with their masses, so the meson mass will not appear in Eqs. (10-13).

Given the chemical potentials μ_B and μ_Q as the input, together with the neutrality condition $\sum_i n_i Q_i = 0$, Eqs. (10-13) form a set of self-consistent nonlinear equations which can be solved numerically. With the Fermi momenta k_i of the particles as the output, we can calculate the energy density and the pressure of the hadronic

matter as:

$$
\begin{aligned}
\rho_H = & \sum_b \frac{f_b c}{16\pi^2\hbar^3}\left[\hbar k_b\sqrt{\hbar^2 k_b^2 + \tilde{m}_b^2 c^2}(2\hbar^2 k_b^2 + \tilde{m}_b^2 c^2)\right. \\
& \left. -\tilde{m}_b^4 c^4 \log\left(\frac{\hbar k_b}{\tilde{m}_b c} + \sqrt{1 + \frac{\hbar^2 k_b^2}{\tilde{m}_b^2 c^2}}\right)\right] \\
& + \frac{1}{2\hbar c}(m_\sigma^2\sigma^2 + m_\omega^2\omega^2 + m_\rho^2\rho^2) \\
& + \sum_l \frac{f_l c}{16\pi^2\hbar^3}\left[\hbar k_l\sqrt{\hbar^2 k_l^2 + m_l^2 c^2}(2\hbar^2 k_l^2 + m_l^2 c^2)\right. \\
& \left. -m_l^4 c^4 \log\left(\frac{\hbar k_l}{m_l c} + \sqrt{1 + \frac{\hbar^2 k_l^2}{m_l^2 c^2}}\right)\right], \qquad (18)
\end{aligned}
$$

$$
\begin{aligned}
p_H = & \sum_b \frac{f_b c}{48\pi^2\hbar^3}\left[\hbar k_b\sqrt{\hbar^2 k_b^2 + \tilde{m}_b^2 c^2}(2\hbar^2 k_b^2 - 3\tilde{m}_b^2 c^2)\right. \\
& \left. +3\tilde{m}_b^4 c^4 \log\left(\frac{\hbar k_b}{\tilde{m}_b c} + \sqrt{1 + \frac{\hbar^2 k_b^2}{\tilde{m}_b^2 c^2}}\right)\right] \\
& - \frac{1}{2\hbar c}(m_\sigma^2\sigma^2 - m_\omega^2\omega^2 - m_\rho^2\rho^2) \\
& + \sum_l \frac{f_l c}{48\pi^2\hbar^3}\left[\hbar k_l\sqrt{\hbar^2 k_l^2 + m_l^2 c^2}(2\hbar^2 k_l^2 - 3m_l^2 c^2)\right. \\
& \left. +3m_l^4 c^4 \log\left(\frac{\hbar k_l}{m_l c} + \sqrt{1 + \frac{\hbar^2 k_l^2}{m_l^2 c^2}}\right)\right]. \qquad (19)
\end{aligned}
$$

The relation between the pressure p and the energy density ρ gives the equation of state, which is shown in Fig. 2, and is subsequently used in the TOV equations to get the stellar structure. The particle densities as a function of baryon density are shown in Fig. 3. Fig. 4 gives the particle composition inside the maximum mass star with the hadronic equation of state ($M = 1.523$ M$_\odot$, $R = 9.72$ km). Remember that the model is used to calculate the equation of state for the whole range of the density, however, this description may not be appropriate near the star surface, i.e., the crust. Nevertheless, the outer crust only affects low mass stars significantly, while we are mainly concerned with maximum mass stars. Furthermore, in view of the cooling behavior, the outer crust has negligible neutrino emissivity compared to the direct Urca process in the core.

Compared to the hadronic phase, the quark phase is more easily described. Quark matter is treated as a free Fermi gas, whereby we assume that asymptotic freedom has taken effect at the very high densities in the center of the star. Thus Eq. (15) is also valid for quarks, where the lepton chemical potential μ_l is substituted with the quark chemical potential μ_q and the degeneracy becomes $f_q = 3 \times (2J_q + 1) = 6$ because of the extra color degrees of freedom. The fact that the quark phase has a different vacuum than the hadronic phase, which has a nonzero expectation value of the gluon field, can be taken into account by the so-called bag model. This model adds a
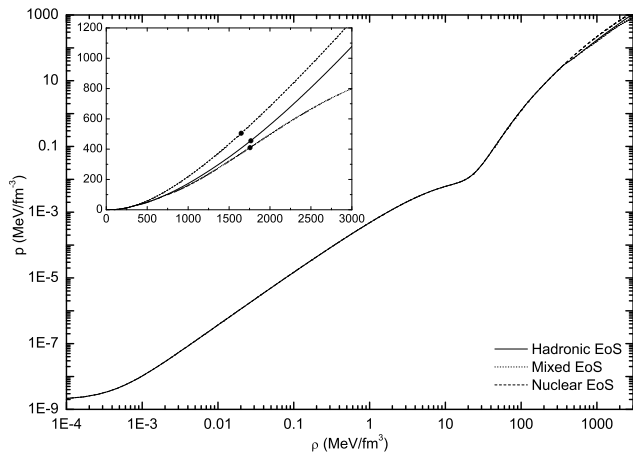
FIG. 2: The equation of state of the various matter phases. The difference only appears at high density as is shown more clearly in the inset, where the dots on the curves indicate the central densities and pressures of the corresponding maximum mass stars.
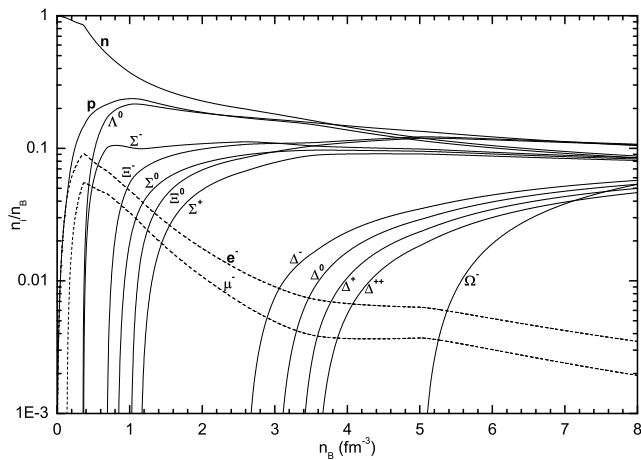

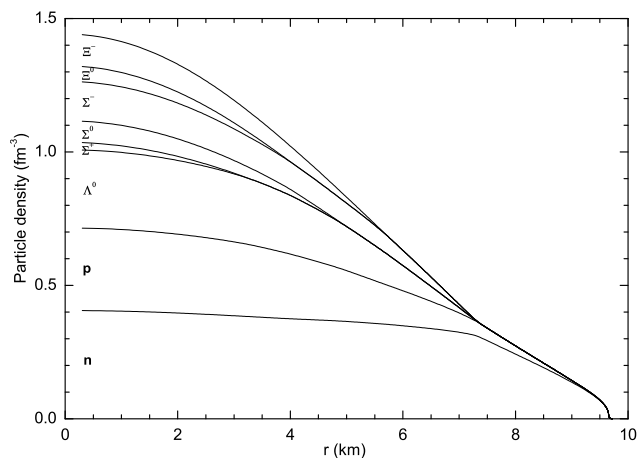FIG. 3: The particle densities n_i/n_B versus baryon density n_B for hadronic matter.

FIG. 4: The particle composition of the maximum mass neutron star with the hadronic equation of state.

constant shift called the bag constant B_c to the pressure and energy density of the quarks, such that

$$\rho_q = \sum_q \frac{f_q}{16c\pi^2\hbar^3}\left[\hbar k_q\sqrt{\hbar^2 k_q^2 + m_q^2 c^2}(2\hbar^2 k_q^2 + m_q^2 c^2)\right.$$

$$\left. - m_q^4 c^4 \log\left(\frac{\hbar k_q}{m_q c} + \sqrt{1 + \frac{\hbar^2 k_q^2}{m_q^2 c^2}}\right)\right]$$

$$+ \sum_l \frac{f_l}{16c\pi^2\hbar^3}\left[\hbar k_l\sqrt{\hbar^2 k_l^2 + m_l^2 c^2}(2\hbar^2 k_l^2 + m_l^2 c^2)\right.$$

$$\left. - m_l^4 c^4 \log\left(\frac{\hbar k_l}{m_l c} + \sqrt{1 + \frac{\hbar^2 k_l^2}{m_l^2 c^2}}\right)\right] + B_c, \qquad (20)$$

$$p_q = \sum_q \frac{f_q}{48c\pi^2\hbar^3}\left[\hbar k_q\sqrt{\hbar^2 k_q^2 + m_q^2 c^2}(2\hbar^2 k_q^2 - 3m_q^2 c^2)\right.$$

$$\left. + 3m_q^4 c^4 \log\left(\frac{\hbar k_q}{m_q c} + \sqrt{1 + \frac{\hbar^2 k_q^2}{m_q^2 c^2}}\right)\right]$$

$$+ \sum_l \frac{f_l}{48c\pi^2\hbar^3}\left[\hbar k_l\sqrt{\hbar^2 k_l^2 + m_l^2 c^2}(2\hbar^2 k_l^2 - 3m_l^2 c^2)\right.$$

$$\left. + 3m_l^4 c^4 \log\left(\frac{\hbar k_l}{m_l c} + \sqrt{1 + \frac{\hbar^2 k_l^2}{m_l^2 c^2}}\right)\right] - B_c, \qquad (21)$$

where the leptons still contribute because the unequal masses of the u, d and s quarks result in unequal densities of these flavors, such that even in the pure quark phase charge neutrality cannot be satisfied without leptons.

As discussed in the introduction, there could also be a mixed phase between the hadronic phase and the quark phase. These two phases are taken to be in equilibrium, i.e., the two phases have the same temperature (both set to zero here), pressure, and chemical potentials. Charge neutrality then determines the volume fraction of these two phases. For the three possible phases (hadronic, quark, and mixed) the system will be in the one with the highest pressure, or equivalently, the lowest grand potential, which determines the phase transition behavior. According to Eq. (21), the bag constant determines the scale at which deconfinement sets in. In other words, the larger the bag constant, the later the quark phase sets in with increasing density. Throughout this paper the bag constant is taken to be $B_c = 230$ MeV/fm^3 unless indicated specifically. In Fig. 5 it is shown how the phase transition takes place between the two phases. Similar to Fig. 3 for the hadronic phase, the various particle densities for the mixed phase are shown in Fig. 6 as a function of baryon density. Fig. 7 shows the particle composition inside the maximum mass star with the mixed equation of state ($M = 1.479$ M$_\odot$, $R = 9.81$ km).

C. Thermal evolution equations

The equations governing the thermal evolution of a spherically symmetric star, given by the metric in Eq.
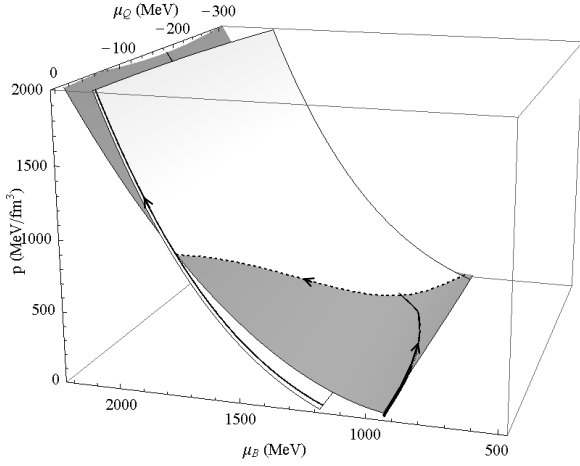
FIG. 5: The pressure surface of the hadronic phase (dark gray) and the quark phase (light gray). The thick solid lines are the neutrality curves in each phase. The thick dashed curve is the intersection of the two pressure surfaces and shows when the two phases are in equilibrium. The arrows indicate how p and μ_Q change with increasing μ_B.
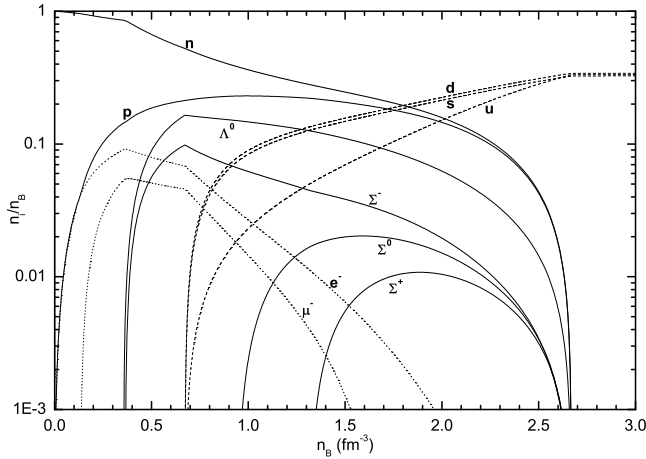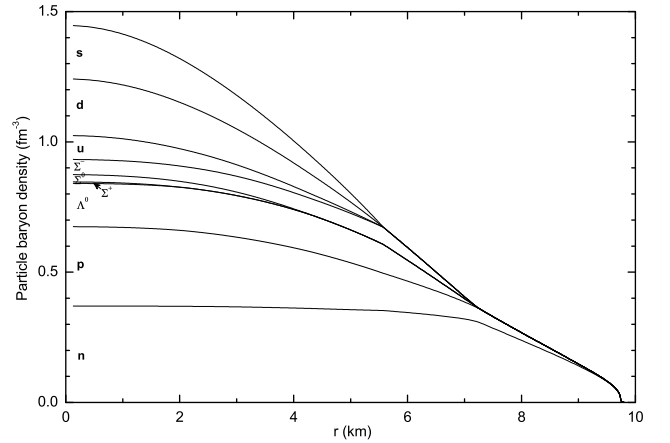

FIG. 7: The particle baryon densities inside the maximum mass neutron star with the mixed equation of state. Note that the quarks have baryon number 1/3.

FIG. 6: The particle densities n_i/n_B versus baryon density n_B for the mixed phase case. The densities of the quarks are expressed in terms of their baryon densities instead of their number densities.

compare with observations, the photon luminosity is of great importance. Here it is assumed to obey the black body radiation law $L_\gamma = 4\pi R^2 q_\gamma = 4\pi\sigma R^2 T_s^4$, where $\sigma = 5.67 \times 10^{-5}$ erg/cm^{2}K^{4}s is the Stefan-Boltzmann constant and T_s is the surface temperature. According to general relativity, an observer at infinity will measure the gravitationally red-shifted temperature and luminosity. The observational quantities are thus $T_\infty = T_s e^{\Phi(R)}$ and $L_\infty = L_\gamma e^{2\Phi(R)}$. As is generally accepted, a very thin layer of the outer crust of the neutron star will act as a thermal insulator causing the temperature at the surface to be much lower than inside the star. The relation between the surface temperature and the inner temperature depends on the chemical composition of this envelop. We will simply locate such a layer at the surface, neglecting its thickness, and adopt the T_∞-T relation given by Potekhin *et al.* [22], as shown in Fig. 8, and set T to be the inside temperature at $r = R$. Note that the surface temperature T_s introduced above is the outside temperature at $r = R$.

The parameters c_V, κ, q_ν and q_γ need to be determined to solve the thermal evolution equations, Eqs. (22) and (23). The specific heat c_V can simply be obtained by summing up all the contributions of the different fermions in the model. In the low-temperature approximation, Fermi-liquid theory gives

$$c_{Vi} = \frac{m_i^* k_i}{3\hbar^2} k_B^2 T, \quad (24)$$

where k_B is Boltzmann's constant, $m_i^* = \hbar k_i/v_i$ is the effective mass on the Fermi surface, and $v_i = d\epsilon_i/(\hbar dk)|_{k=k_i}$ is the Fermi velocity of quasi-particle i. For leptons the effective mass is easily obtained since they are described as a free Fermi gas, i.e., $m_l^* = \sqrt{\hbar^2 k_l^2/c^2 + m_l^2} = \mu_l/c^2$. Similarly for quarks, $m_q^* = \mu_q/c^2$. For baryons the effective mass follows from the

(6), are [21]:

$$c_V \frac{\partial(Te^\Phi)}{\partial t} = -\frac{e^{-\lambda}}{4\pi r^2}\frac{\partial(Le^{2\Phi})}{\partial r} - q_\nu e^{2\Phi} - q_\gamma e^{2\Phi}, \quad (22)$$

$$\kappa\frac{\partial(Te^\Phi)}{\partial r} = -\frac{Le^{\lambda+\Phi}}{4\pi r^2}, \quad (23)$$

where c_V is the specific heat capacity at constant volume, κ is the thermal conductivity, q_ν and q_γ are the neutrino and photon emissivity, respectively. The photon emissivity q_γ is only nonzero on the surface $r = R$. It is convenient to define the redshifted temperature $\tilde{T} = Te^\Phi$ inside the star. Similarly, $Le^{2\Phi}$ represents the redshifted luminosity corresponding to the heat current. In order to

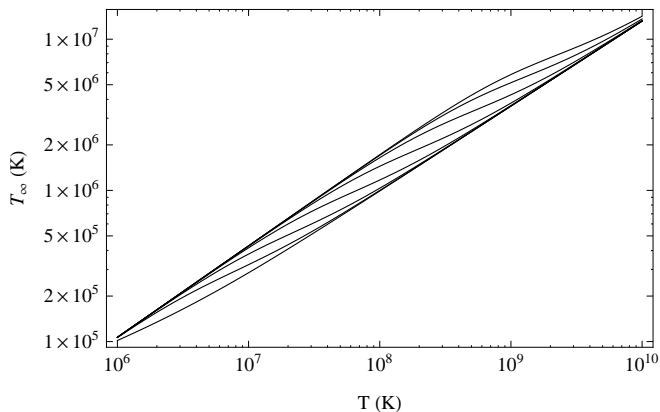FIG. 8: The T_∞-T relation for different numbers of light elements parameterized by $\eta = g_{14}^2 \Delta M_l/M$, where ΔM_l is the mass of the light elements in the envelop and g_{14} is the surface gravity in unit of 10^{14} cm/s^2 [22], the different curves correspond to $\log \eta = -\infty, -16, -14, -12, -10, -8, -6$ and 0 from bottom to top, respectively. These results are for the maximum mass neutron star with the hadronic equation of state, where $g_{14} = 2.918$.

dispersion relation in Eq. (14)

$$v_b = \left.\frac{d\epsilon_b(k)}{\hbar dk}\right|_{k=k_b} = \frac{\hbar k_b}{\sqrt{\hbar^2 k_b^2/c^2 + \tilde{m}_b^2}}, \qquad (25)$$

such that $m_b^* = \sqrt{\hbar^2 k_b^2/c^2 + \tilde{m}_b^2}$. The effect of interactions is, in the mean-field approximation, only present in the reduced mass $\tilde{m}_b$ of the baryons.

The general expression for the neutrino emissivity has the form $q_{\nu i} = C_i T^s$, where C_i and s are different constants for each kind of process. For the direct Urca process we have $s = 6$ and for the modified Urca process $s = 8$. The difference in the exponents shows the inefficiency of the modified Urca process since the temperature T of a neutron star is much smaller than the typical Fermi temperature T_F. The neutrino emissivities for the various processes are summarized in Ref. [3]. For the general baryon direct Urca process, cf. Eq. (4), the emissivity is

$$q_{\nu 12l} \approx 1.207 \times 10^{25} \frac{\mu_l m_{b1}^* m_{b2}^*}{(1 \text{ MeV}) m_n^2} R_{12} T_9^6 \Theta_{12l} \text{ erg/cm}^3\text{s}, \qquad (26)$$

where T_9 is the temperature in units of 10^9 K, Θ_{12l} is 1 only if the Fermi momenta of the two baryons b_1, b_2 and the lepton l can form a triangle, otherwise $\Theta_{12l} = 0$. The coefficients R_{12} vary depending on the baryons involved in the process. In our mean-field model the maximum mass star contains massive hyperons up to Ξ, such that all possible direct Urca processes given in Ref. [23] need to be included, as listed in Table II. For the quark direct

TABLE II: The coefficients R_{12} for different direct Urca processes [23], denoted by the baryons involved in each process.

np	$\Lambda^0 p$	$\Sigma^- n$	$\Sigma^- \Lambda^0$	$\Sigma^- \Sigma^0$	$\Xi^- \Lambda^0$	$\Xi^- \Sigma^0$	$\Xi^0 \Sigma^+$	$\Xi^- \Xi^0$
1	0.0394	0.0125	0.2055	0.6052	0.0175	0.0282	0.0564	0.2218

Urca emissivities, we refer to Ref. [24]:

$$q_{\nu u dl} \approx 4.773 \times 10^{18} \frac{\hbar^2 c^2 [(k_u + k_l)^2 - k_d^2] \mu_d}{1 \text{ MeV}^3} T_9^6 \text{ erg/cm}^3\text{s},$$

$$q_{\nu u sl} \approx 2.552 \times 10^{17} \frac{\hbar^2 c^2 [(k_u + k_l)^2 - k_s^2] \mu_s}{1 \text{ MeV}^3} T_9^6 \text{ erg/cm}^3\text{s},$$

$$\qquad (27)$$

where the efficiency of the strange quark channel is reduced because it changes strangeness. Since the direct Urca channels are open, it is not necessary to consider other neutrino-emission processes.

In the present model, the thermal conductivity κ cannot be easily obtained since it strongly depends on the interactions between the particles in the complicated hadronic phase. For the mixed case, the interface between the phases may introduce even more uncertainty. Therefore, the thermal relaxation period inside the star is not considered here and the calculation simply starts when the star has become isothermal, as indicated in the introduction. Because of this simplification the interesting early stage behavior of the cooling cannot be discussed. This disadvantage may also be one of the reasons why such hadronic models are not extensively studied. However, the typical thermal relaxation time is usually less than a century and most of the available observational data is of the later stages, i.e., after the star has become isothermal, such that the results obtained after the relaxation period has ended are still useful. Consequently, the star will be treated as an isothermal object with a constant temperature $\tilde{T}$ and the equations are rather simplified. Instead of two coupled partial differential equations in Eqs. (22) and (23), we have now only one ordinary differential equation:

$$C_V \frac{d\tilde{T}}{dt} = -Q_\nu - L_\infty, \qquad (28)$$

where the capital letters represent the integrated parameters over the volume of the star, namely

$$C_V = 4\pi \tilde{T} \sum_i \int_0^R \frac{\bar{c}_{Vi}(r) e^{\lambda(r)} r^2}{e^{\Phi(r)}} dr, \qquad (29)$$

$$Q_\nu = 4\pi \tilde{T}^s \sum_i \int_0^R \frac{\bar{q}_{\nu i}(r) e^{\lambda(r)} r^2}{e^{(s-2)\Phi(r)}} dr, \qquad (30)$$

where the T-dependent parts are taken outside of the radial integral and the temperature-independent prefactors of c_{Vi} and $q_{\nu i}$ are denoted with a bar. The factors of $e^{\Phi(r)}$ in the denominators are a consequence of the construction of the isothermal temperature $\tilde{T}$. Note that

the isothermal temperature does not take into account the temperature decrease near the surface of the star, which occurs in a very thin layer close to the surface.

The total heat capacity and the neutrino emissivities for both the direct and modified Urca processes as a function of the radial coordinate are shown in Figs. 9 and 10 for the case of a maximum mass neutron star with the hadronic and mixed equations of state, respectively. Here "total" means summed over all particles which contribute, but not integrated over the star volume. The quantities were obtained at $T = 10^9$ K, but the values at different temperatures can be obtained directly from the temperature dependence of c_V and q_ν. The discontinuities in the emissivity are due to the step functions in the expressions for the emissivities. These step functions are a consequence of the low-temperature approximation, which does not take into account any further momentum fluctuations around the Fermi surfaces. Also q_{MUrca} is calculated only for the nucleon processes shown in Eq. (3) with the following emissivity [3]:

$$q_{\nu Mn} \approx 1.882 \times 10^{19} \frac{m_n^{*3} m_p^* \hbar^2 c^2 k_p k_l}{(1\ \mathrm{MeV})\mu_l m_n^3 m_p} T_9^8 \ \mathrm{erg/cm^3 s},$$

$$q_{\nu Mp} \approx \left(\frac{m_p^*}{m_n^*}\right)^2 \frac{(3k_p + k_l - k_n)^2}{8 k_p k_l} \Theta_{Mp} q_{\nu Mn}, \qquad (31)$$

where the subscript Mn or Mp means the process is modified by a bystander neutron n or proton p, and Θ_{Mp} is 1 only if $3k_p + k_l > k_n$ as required by momentum conservation in the Mp process. The modified Urca processes are only calculated when the nucleon direct Urca process is forbidden, since the formulae are only valid in this case. The small region of overlap where both q_{DUrca} and q_{MUrca} are nonzero is due to the different thresholds for the direct Urca processes with electrons e^- and muons μ^-.

III. NUMERICAL RESULT

In this section the three different equations of state for the hadronic matter, the mixed phase of hadronic and quark matter, and nuclear matter are compared. Since the maximum masses are not very large for the last two cases, we concentrate on the star with the maximum allowable mass for each equation of state. The initial temperature is always set as $\tilde{T} = 10^9$ K at $t = 0$, which corresponds to the time at which the isothermal condition is reached. As mentioned previously, the thermal relaxation period is not included in our calculation, which is about several decades according to calculations with nuclear matter [3]. The results are plotted in a logarithmic time scale, such that our results can be shown directly with most of the observational data even though the data include the thermal relaxation era of the neutron stars, that is negligible compared to the age of the stars. However, this makes it hard to draw a comparison with the recent observation of the cooling of the Cassiopeia A
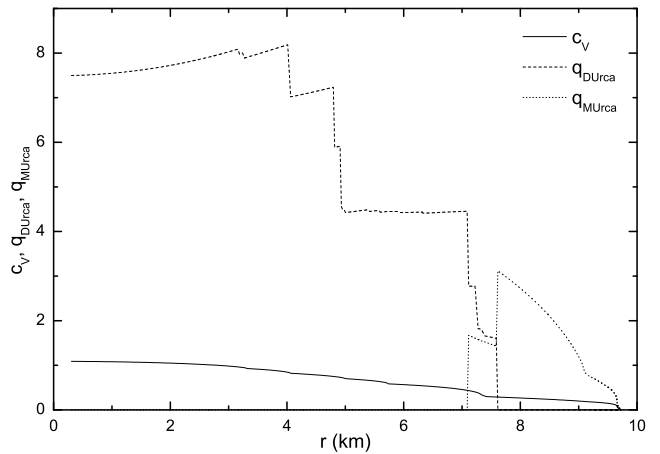

FIG. 9: The total heat capacity (c_V) and the neutrino emissivities of the direct Urca (q_{DUrca}) and modified Urca (q_{MUrca}) processes inside the neutron star with the hadronic equation of state at $T = 10^9$ K. Here, c_V is in units of 10^{21} erg/cm^{3}K, q_{DUrca} is in units of 10^{27} erg/cm^{3}K, and q_{MUrca} is in units of 10^{19} erg/cm^{3}K.
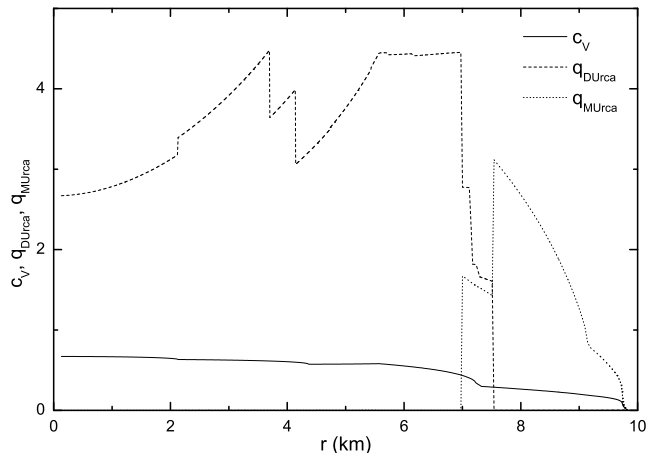

FIG. 10: The same as in Fig. 9 but now for the mixed equation of state.

neutron star [25], which provides direct evidence for the cooling process. This neutron star is too young and is believed to have become isothermal quite recently, such that the thermal relaxation period is not negligible.

In order to avoid confusion, our results always show cooling curves starting at $t = 1$ yr, when the result has become not very sensitive to the initial conditions. In fact, the effect of the initial temperature is limited to the very beginning. The higher the initial temperature is, the faster the dependence dies away, which can be seen clearly from the asymptotic temperature dependence of the neutrino-emission dominated era

$$\tilde{T} = \left[\frac{(s-2)Q_0}{C_0} t + \tilde{T}(0)^{2-s}\right]^{\frac{1}{2-s}}, \qquad (32)$$

where C_0 and Q_0 are the constant coefficients of the $\tilde{T}$-

dependent factors in Eqs. (29) and (30). This asymptotic solution can be easily obtained by dropping the photon radiation term in Eq. (28) and keeping only the leading neutrino-emission process with the smallest exponent s. Note that the exponent s is never smaller than 6 for any of the neutrino-emission processes. It is quite clear that the late-time behavior of the neutrino-emission dominated era is thus completely determined by the coefficients of the heat capacity and the neutrino emissivity and not by the initial condition $\tilde{T}(0)$.

For the hadronic equation of state, Fig. 11 shows the evolution of the temperatures $\tilde{T}$ and T_∞, where it can be seen that the cooling process can be divided into two stages, namely the neutrino-emission dominated and photo-radiation dominated era. The two eras can be clearly seen from the energy loss due to the different processes as shown in Fig. 12, where the switch from neutrino emission to photon radiation occurs at $t \approx 3 \times 10^4$ yr. In Fig. 12 the energy emission due to the modified Urca processes is also shown demonstratively by considering only the processes involving the nucleons in Eq. (3). This, of course, underestimates the energy loss due to the modified Urca processes, however, the magnitude is expected to be of the same order. The energy loss by these processes is seen to be less than 10^{-9} of the total energy loss, such that the modified Urca processes are always negligible in the present calculation. In Figs. 11 and 12 the T_∞-T relation is used with $\eta = 10^{-10}$. It is found that different values of η only slightly change the cooling process, as shown in Fig. 13, where two groups of cooling curves with extremely large and almost vanishing η are compared. The difference is that, for the neutrino-emission dominated era, T_∞ can differ by about a factor of 2 but the inner temperature is almost not influenced. With less massive elements in the envelop, i.e., smaller η, the turning point into a photon-radiation dominated era is a little sharper and the final temperatures are a little lower. In any case, these effects are not very significant and can hardly be distinguished with the present accuracy of observational data. Without loss of generality, the value $\eta = 10^{-10}$ will be used in this section. Here we should also point out that the calculation cannot be carried out after $\tilde{T}$ is smaller than 10^4 K, because then the T_∞-T relation given in Ref. [22] is no longer valid.

The thermal evolution of the neutron star with the mixed equation of state is shown in Fig. 14, which is similar to the purely hadronic case. The straight lines represent the asymptotic behavior, which are solved using Eq. (28) by neglecting Q_γ or Q_ν for the neutrino-emission dominated or photon-radiation dominated era, respectively. For example, in the neutrino-emission dominated era, for the hadronic equation of state the temperatures scale with time as $\tilde{T} \sim 1.6 \times 10^9 \ (t/\mathrm{yr})^{-1/4}$K, $T_\infty \sim 1.1 \times 10^7 \ (t/\mathrm{yr})^{-0.602/4}$K, where the power 0.602 comes from the asymptotic approximation for the T_∞-T relation at low temperature, $T_\infty \propto T^{0.602}$. For the mixed phase, the temperature scalings are just slightly higher: $\tilde{T} \sim 1.77 \times 10^9 \ (t/\mathrm{yr})^{-1/4}$K, $T_\infty \sim 1.13 \times$
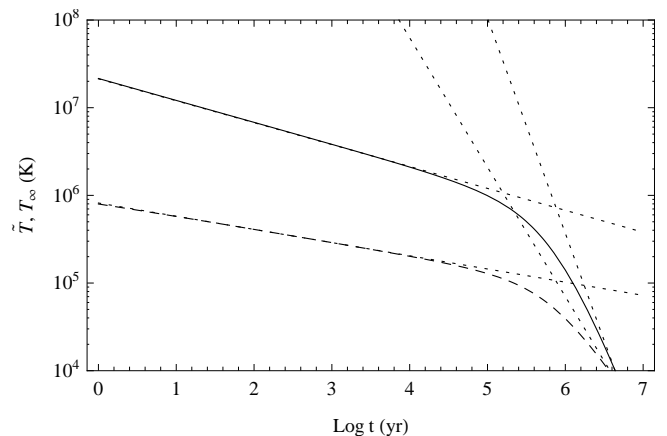

FIG. 11: The temperature evolution of the neutron star with the hadronic equation of state. The solid curve represents $\tilde{T}$ while the dashed curve represents T_∞, with the dotted straight lines indicating the asymptotic behavior.
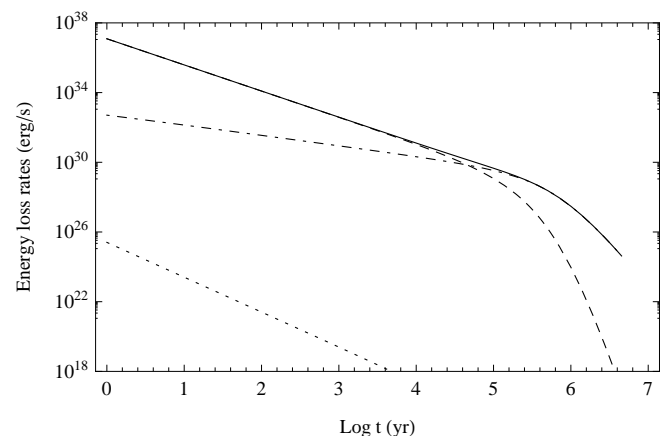

FIG. 12: The energy lost by different processes in the neutron star with the hadronic equation of state, where the solid curve is the total energy loss rate, the dashed curve is the energy loss due to direct Urca neutrino emission, the dotted curve is due to modified Urca neutrino emission, and the dot-dashed curve is due to photon radiation.

$10^7 \ (t/\mathrm{yr})^{-0.602/4}$K. This is due to the fact that the thermal parameters, after being integrated over the whole star, are not quite different for the two cases even though the stars have different structure and mass. For example, for the hadronic case we have $C_V = 3.331 \times 10^{39}\tilde{T}_9$ erg/K and $Q_\nu = 1.227 \times 10^{47}(\tilde{T}_9)^6$ erg/s, while for the mixed phase $C_V = 2.839 \times 10^{39}\tilde{T}_9$ erg/K and $Q_\nu = 7.280 \times 10^{46}(\tilde{T}_9)^6$ erg/s. To demonstrate the effect of the mixed phase, the same curves are shown in Fig. 15 with a smaller bag constant of $B_c = 170$ MeV/fm^3, where we see that it causes a slightly higher temperature. As pointed out earlier, a smaller bag constant causes the deconfined phase of quarks to appear at lower densities, such that the volume of the mixed phase is increased. In this case we find $C_V = 2.156 \times 10^{39}\tilde{T}_9$ erg/K and
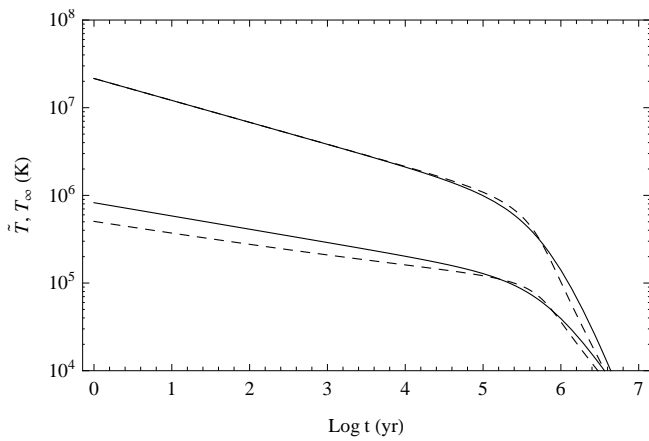
FIG. 13: The temperature evolution of the neutron star with the hadronic equation of state with different T_∞-T relation. The solid curves correspond to $\eta = 1$ while the dashed curves correspond to $\eta = 10^{-20}$. The upper group is $\tilde{T}$ and the lower group is T_∞.
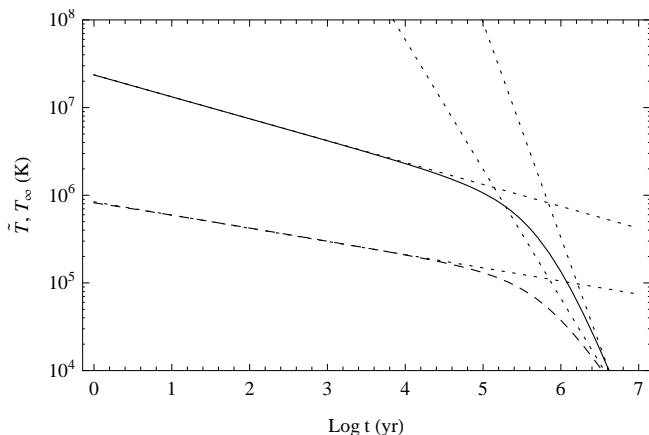

FIG. 14: The same as in Fig. 11 but with the mixed equation of state.

FIG. 15: The same as in Fig. 14 but with $B_c = 170 \text{MeV/fm}^3$.
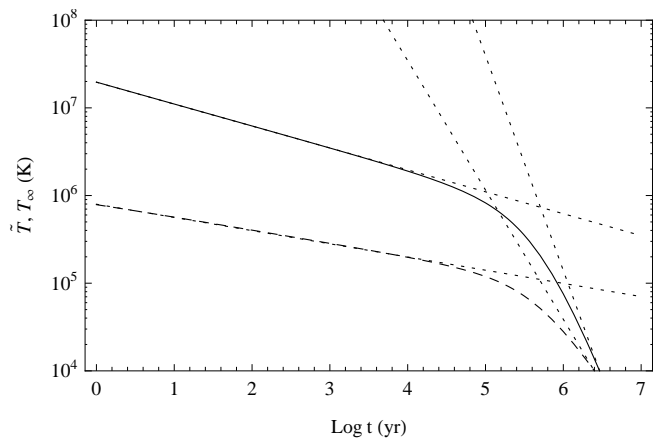
FIG. 16: The same as in Fig. 11 but with the nuclear equation of state.

$Q_\nu = 2.590 \times 10^{46} (\tilde{T}_9)^6$ erg/s. Nevertheless, the total effect on the cooling process is not drastically changed. According to these results, we expect that even if the mixed phase is reduced because of screening and surface effects, the cooling behavior is not changed considerably.

For the nuclear equation of state, the maximum mass is 1.719 M$_\odot$ with $R = 10.04$ km and its thermal evolution is shown in Fig. 16. To summarize, the luminosity for the three types of equations of state are plotted in Fig. 17, where a comparison with observational data is also made. In all three cases the cooling is too fast compared with the data. The star with the nuclear equation of state cools a little faster, since the direct Urca processes with hyperons in the hadronic phase and the mixed phase are not as efficient as the nucleon direct Urca process [23]. However, the difference is quite small such that it might be hard to distinguish these different equations of state
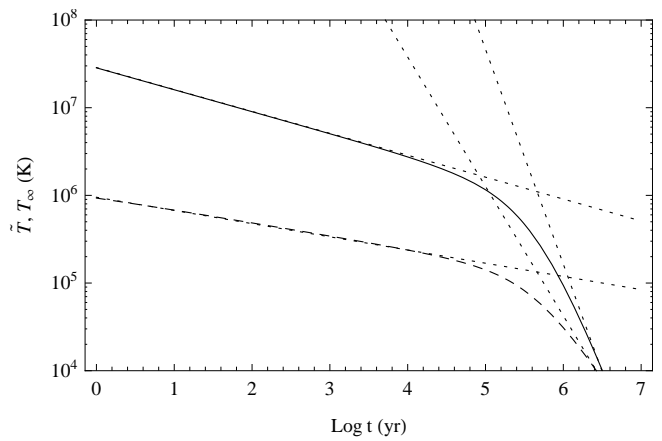
simply by their thermal evolution after the isothermal condition is reached.

IV. EFFECT OF SUPERFLUIDITY

From the above results, we can see that our neutron stars cool too fast because the direct Urca process is open for all the three types of equations of state. An explanation could be that the neutrino emissivity is overestimated by neglecting the possibility of superfluidity. As pointed out in the introduction, it is generally believed that superfluidity appears inside neutron stars due to the attractive part of the nuclear force, for both the nucleons and the hyperons. Due to the presence of an energy gap Δ, associated with the binding energy of the Cooper pairs, the number of excitations near the Fermi surface are suppressed by a factor of $\exp(-\Delta/k_B T)$ when the temperature is smaller than a certain critical temperature T_c. Therefore, pairing reduces the heat capacity and the neutrino emissivity significantly when the star cools down to temperatures below T_c, thus the cooling
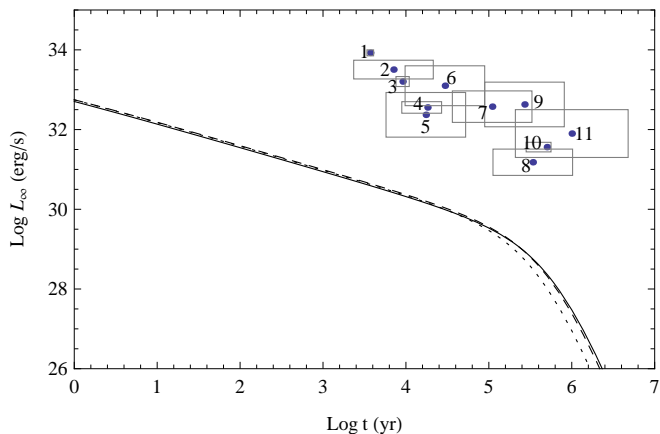
FIG. 17: The luminosity of neutron stars with different equations of state, with solid, dashed, and dotted curves representing the hadronic, the mixed, and the nuclear equation of state, respectively. The observational data are from Ref. [26], with the numbers indicating the corresponding stars as: 1 - RX J0822-4247, 2 - 1E 1207.4-5209, 3 - RX J0002+6246, 4 - PSR 0833-45 (Vela), 5 - PSR 1706-44, 6 - PSR 0538+2817, 7 - PSR 0656+14, 8 - PSR 0633+1748 (Geminga), 9 - PSR 1055-52, 10 - RX J1856.5-3754, and 11 - RX J0720.4-3125.

behavior is drastically changed. In this section we will explore the effect of superfluidity to the cooling process of neutron stars.

A. Superfluidity inside neutron stars

In our present model for neutron stars, there are different fermions, namely the baryons, the leptons, and the quarks. The typical T_c of baryons is about $0.1 - 1$ MeV, which is close to the initial temperature of neutron stars, such that the superfluidity of baryons is very important to the cooling process. As for the leptons, such as electrons, they could become superfluid due to interactions via phonons, however, the typical T_c is very small, namely in the order of several kelvin. Hence lepton superfluidity is expected to be unimportant to the neutron star cooling process. For quarks in the mixed phase, the gaps can be about $50 - 100$ MeV [12], which is much higher than the typical temperatures of the stars we are concerned with. The quark contribution will thus be suppressed more strongly than the baryonic contribution. Without superfluidity the quark contributions to the heat capacity and the neutrino emissivity were shown to be of the same order as the baryonic ones, such that with superfluidity they are completely negligible at the same stellar temperature. Throughout this section we thus only consider the contributions to c_V and q_ν of non-superfluid leptons and superfluid baryons but neglect those of the superfluid quarks.

Superfluidity not only reduces the neutrino emissivity but also opens a different channel of neutrino emission based on the breaking and formation of Cooper pairs. At temperatures not far below T_c thermal fluctuations can cause pair break-up into single-particle excitations, which subsequently reform into pairs. Neutrino emission due to such processes is quite efficient at temperatures slightly below T_c and can even surpass the direct Urca process in some cases [27]. However, its contribution also decreases dramatically when T becomes small due to the exponential reduction factor mentioned previously. According to a similar argument as above, we only need to consider such neutrino-emission processes involving baryon pairs.

By taking into account superfluidity, the dominant neutrino-emission process is no longer simply determined by the density, which is crucial for the threshold of the direct Urca process, but also depends on the reduced temperature $\tau = T/T_c$. However, it is still true that the modified Urca process can be neglected as long as the direct Urca process is open, since the modified Urca process involves more particles and is more strongly suppressed due to the energy gaps of all superfluid participants. Thus we again do not consider the modified Urca process since the direct Urca process is always open in our study. According to Ref. [27] electron-electron bremsstrahlung becomes a dominant process when all baryons are strongly superfluid at low temperature. So for a correct estimate of the neutrino emission at low temperatures we also include lepton-bremsstrahlung processes. Based on the discussion above, in order to include the effect of superfluidity we should recalculate c_V and q_ν for all baryons, neglect those of the quarks in the mixed phase, keep the lepton contributions unchanged, and also include the newly introduced neutrino emission due to baryon pair break-up and lepton bremsstrahlung. We next discuss these effects separately.

To describe the superfluidity of the particles, it is necessary to specify the type of pairing. At low density, the singlet-state nuclear interaction is attractive, while at higher densities it becomes repulsive. It is believed, however, that the triplet-state interaction still provides an attractive channel at high densities, such that triplet-state pairing is expected in the core of the neutron star. This transition happens around the nuclear saturation density $n_0 = 0.16$ fm^{-3}. The proton pairing is usually taken to be in the singlet channel, even in the stellar core, due to their low concentration. However, in our model, as seen from Figs. 4 and 7, the densities of neutrons and protons in the core are quite close to each other, namely $n_p \sim 0.2 - 0.3$ fm^{-3} and $n_n \sim 0.4$ fm^{-3}. It thus seems that both the protons and the neutrons should form triplet-state pairs. The hyperons, which can also become superfluid, are usually taken to pair in the singlet channel. But in our model there are some hyperons, e.g. Λ^0, which can have densities comparable to the neutrons and protons. As was discussed earlier, the details of the interactions between the hyperons are not well established and thus there are some ambiguities in dealing with hyperons with largely varying densities. For the singlet-state pairing of neutrons, protons [26], and Λ^0's [28] the results of many models largely agree on the order

of magnitude of the pairing gaps and their density dependence. As discussed, triplet-state pairing is of great interest to our model, however, there is little known about this kind of pairing except for the case of neutrons for which it is still highly model dependent. In fact, the existence of triplet-state pairing inside neutron stars is still uncertain. According to observations of the cooling neutron stars, it seems necessary to have *all* baryons in the superfluid state. For example, the effect of superfluidity on the thermal evolution of neutron stars with hyperons in the core has been studied by Schaab *et al.* [29], which only included the singlet-state pairing of Λ^0 at low densities but did not include the triplet-state pairing of Λ^0 at high densities and ignored the pairing of other hyperons. The cooling was found to be too fast for heavy stars since not all the direct Urca processes were suppressed.

To estimate the effect of superfluidity, we make the simplifying assumption that, regardless of the density, the neutrons, protons, and Λ^0's pair in the triplet channel, the remaining hyperons pair in the singlet channel, and the critical temperatures of all the baryons are taken to be equal. Equating all critical temperatures of the various baryons is consistent with our model, since all baryons couple equally to the meson fields. Although our pairing mechanism seems quite crude, we expect that, at least qualitatively, the effect of pairing on the thermal evolution of the star will be taken into account. To discuss our simplifications, we first need to go into the details of how the specific heat and neutrino emissivity are reduced by superfluidity.

1. Reduction factor

The new expressions for c_V or q_ν are easily obtained by multiplying the original expressions by a reduction factor R_c or R_q. These reduction factors are functions of the reduced temperature τ and also depend on the type of superfluidity considered. A rather systematic calculation of these reduction factors has already been carried out (see review [27] and references therein). In general, the different types of triplet-state pairing can be represented by the projections $m_J = 0, \pm 1, \pm 2$ of the total angular momentum. We only present the most studied $m_J = 0$ case, which is denoted as type-B pairing. Singlet-state pairing is referred to as type A. By introducing the dimensionless variables $\tau = T/T_c$ and $v(\tau) = \Delta(T)/k_B T$, the properties of superfluidity can be described independent of T_c. Numerical fits for the energy gap are given by

$$v_A = \sqrt{1-\tau}\left(1.456 - \frac{0.157}{\sqrt{\tau}} + \frac{1.764}{\tau}\right), \quad (33)$$

$$v_B = \sqrt{1-\tau}\left(0.7893 + \frac{1.188}{\tau}\right), \quad (34)$$
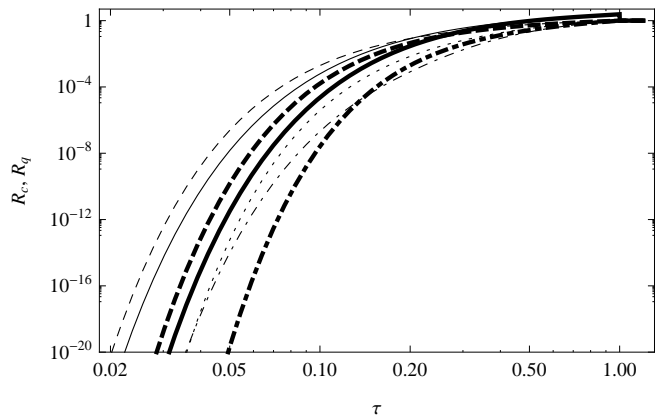

FIG. 18: The reduction factors R_c (solid curves) and R_q (dashed curves) for different types of superfluidity, where type-A (thick curves) is always lower than type-B (thin curves) pairing. Notice the jump of R_c at $\tau = 1$. The dotted curve represents R_{qB}^2 used for the direct Urca process where both baryons are superfluid and have the same T_c. Also R_{qAA} [30] (dot-dashed curve) and R_{qA}^2 (thick dot-dashed curve) are shown for comparison.

and $v \equiv 0$ at $\tau > 1$. The reduction factors for c_V are

$$R_{cA} = \left(0.4186 + \sqrt{1.014 + 0.2510v_A^2}\right)^{2.5}$$
$$\times e^{1.456 - \sqrt{2.120 + v_A^2}}, \quad (35)$$

$$R_{cB} = \left(0.6893 + \sqrt{0.6241 + 0.07975v_B^2}\right)^{2}$$
$$\times e^{1.934 - \sqrt{3.740 + v_B^2}}. \quad (36)$$

Notice that $R_{cA} = 2.426$ and $R_{cB} = 2.188$ are greater than 1 at $\tau = 1$, such that the specific heat is discontinuous as the temperature falls below T_c. The neutrino emissivity for the direct Urca process is different if both or only one of the two involved baryons is superfluid. For the case with only one superfluid baryon

$$R_{qA} = \left(0.2312 + \sqrt{0.5911 + 0.02068v_A^2}\right)^{5.5}$$
$$\times e^{3.427 - \sqrt{11.74 + v_A^2}}, \quad (37)$$

$$R_{qB} = \left(0.2546 + \sqrt{0.5556 + 0.01649v_B^2}\right)^{5}$$
$$\times e^{2.701 - \sqrt{7.295 + v_B^2}}. \quad (38)$$

Generally, type-A pairing always has a stronger reduction effect than type B, as shown in Fig. 18.

The reduction factor for the case where both particles are superfluid is not simply the product of the two reduction factors of each particle, due to different phase-space restrictions. This was pointed out in Ref. [30], where the authors presented the numerical fits for the reduction factors for the AA and BA cases. Here the cases are

distinguished by the type of pairing (A or B) of the neutrons and protons, labeled as AA, BA or BB, where the first letter signifies the type of pairing for the neutrons and the second the pairing type for the protons. We do not present their complicated expressions here. The most important factor we need is for the BB case, which as far as we know has not been explicitly calculated yet. Therefore, we use $R_{qB}(\tau_1)R_{qB}(\tau_2)$ instead of $R_{qBB}(\tau_1, \tau_2)$ for those direct Urca processes with both baryons paired in the triplet-state, which we refer to as the standard setting. Furthermore, we even use this expression for *all* the direct Urca processes with two superfluid baryons, independent of the pairing type. Therefore, the effect of superfluidity on the emissivity for the BB-type process is expected to be overestimated [27]. On the other hand, since the above substitution is also applied to the n, p and Λ^0 at lower densities and other hyperons, which are supposed to pair in the singlet channel, the suppression will be underestimated in these cases. The errors in these two approximations thus work in opposite direction and roughly reduce the total error of our calculation. The reduction factors of the direct Urca process with two superfluid baryons are compared in Fig. 18. It is seen that their differences can become very large for $T \ll T_c$. However, in this case the reduction factors are extremely small and the lepton-bremsstrahlung processes are expected to be dominant, such that in this regime any ambiguity due to the type of pairing is expected to be unimportant.

2. New neutrino emission processes due to superfluidity

The neutrino emissivity associated with Cooper pair break-up is given by [31]

$$q_{\nu b}^C = 1.17 \times 10^{21} N_\nu \frac{m_b^* \hbar k_b}{m_n^2 c} a_b F(v) T_9^7 \text{ erg/cm}^3\text{s}, \quad (39)$$

where $N_\nu = 3$ is the number of neutrino flavors, a_b is a numerical factor from the electroweak neutral currents and depends on the quark composition of the baryon and the pairing type. As far as we know, no calculation has been carried out which included the triplet-state pairing of Λ^0. We simply use $a_\Lambda = a_n$, considering that the quark composition of Λ^0 is similar to the neutron with one d quark replaced by one s quark, while their contributions to the neutral current are the same. This treatment is different from the approximation in Ref. [32], where the contribution from quarks other than u and d is neglected. This may cause some uncertainties, but what matters in the cooling process is the order of magnitude of each process. Since a_b appears as a multiplier rather than an exponent in Eq. (39), such an inaccuracy will not be magnified during the calculation. In fact, we will see that due to the assumption of a uniform T_c, the neutrino emission associated with Cooper pair break-up is always negligible compared to the direct Urca process even if the suppression due to superfluidity is included. The factor

TABLE III: The factor a_b of the neutrino emissivity due to the Cooper pair break-up of the various particles [31]. Notice that we take the coefficient of Λ^0 to be the same as n, which differs from Refs. [31, 32].

	triplet-state			singlet-state			
baryon	p	n	Λ^0	$\Sigma^\pm$	Σ^0	Ξ^0	Ξ^-
a_b	3.18	4.17	4.17	1.17	0	1	0.0064

a_b for the various baryons used in the calculation is shown in Table III.

The function $F(v)$ plays the same role as the reduction factor and is fitted in Ref. [31] to:

$$F_A = (0.602v_A^2 + 0.5942v_A^4 + 0.288v_A^6)\left(0.5547 + \right.$$
$$\left. \sqrt{0.1983 + 0.0113v_A^2}\right)^{1/2} e^{2.245 - \sqrt{5.04 + 4v_A^2}}, \quad (40)$$

$$F_B = \frac{1.204v_B^2 + 3.733v_B^4 + 0.3191v_B^6}{1 + 0.3511v_B^2}\left(0.7591 + \right.$$
$$\left. \sqrt{0.05803 + 0.3145v_B^2}\right)^2 e^{0.4616 - \sqrt{0.2131 + 4v_B^2}}. \quad (41)$$

Furthermore, the neutrino emissivity due to the lepton-bremsstrahlung process ee is given by [33]

$$q_\nu^{ee} = 2.089 \times 10^{11} \frac{\hbar c k_e}{1\text{MeV} y_s} T_9^8 \text{ erg/cm}^3\text{s}, \quad (42)$$

where y_s is a dimensionless parameter representing the effect of screening in the plasma, $y_s = k_{sc}/2k_e$, with k_{sc} the screening wavenumber. This wavenumber is obtained for the case of static screening in the limit of zero temperature [34] by the Thomas-Fermi expression:

$$k_{sc}^2 = \frac{4e^2}{\pi \hbar^2}(\sum_l m_l^* k_l + \sum_b m_b^* k_b Z_b), \quad (43)$$

where the summation over b is over all charged baryons, and Z_b represents the effect of superfluidity on the baryons. Since lepton bremsstrahlung only becomes important if all the baryons are highly superfluid, for which Z_b becomes negligibly small compared to the lepton terms, we can simply omit the terms related to the baryons. Subsequently, y_s is simplified to

$$y_s = \sqrt{\frac{\alpha \mu_Q \sum_l k_l}{\pi \hbar c k_e^2}}, \quad (44)$$

where α is the fine-structure constant. Other processes involving non-relativistic muons are calculated in Ref. [33]. In our model the muons are relativistic, so we adopt the similarity criterion [3] and get

$$q_\nu^{e\mu} = 4\frac{k_\mu}{k_e}q_\nu^{ee}; \quad q_\nu^{\mu\mu} = \frac{k_\mu^2}{k_e^2}q_\nu^{ee}. \quad (45)$$
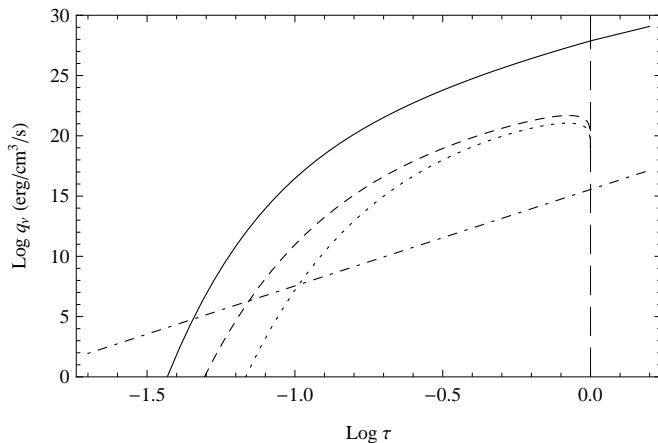
FIG. 19: The neutrino emissivities of the various processes at different temperatures. The solid curve is for the direct Urca process, the dashed curve for the triplet-pair break-up process, the dotted curve is for the singlet-pair break-up process, while the dot-dashed curve for the lepton-bremsstrahlung process. The vertical dashed line at $\tau = 1$ indicates the onset of superfluidity of all baryons. The emissivities are calculated at the central density of the maximum mass neutron star with the hadronic equation of state and $T_c = 10^9$ K.

To summarize, in Fig. 19 we present the neutrino emissivities of the discussed processes as a function of reduced temperature τ after the inclusion of superfluidity. Due to our assumption of equal T_c, the emissivity associated with Cooper pair break-up is always about 5 orders of magnitude smaller than for the direct Urca process. This agrees qualitatively with the result in Ref. [27] for the equal T_c case of nuclear matter. For the neutron star with the mixed equation of state, the situation is similar since the leading contribution of triplet-state paired baryons changes very little. In fact, we can always neglect the contribution to the neutrino emissivity associated with Cooper pair break-up.

Finally, it should be pointed out that superfluidity can also affect the equation of state. However, the equation of state used in the TOV equations is an integral over all states in momentum space and it is expected that the effect of the energy gap at the Fermi surface is very small for very high densities. Therefore, we can still use the stellar structure obtained from the previous unaffected equation of state. Again, we only present the results from the maximum mass star for each type of equation of state.

B. Numerical results

The calculation of the thermal evolution of the star is similar to the case without superfluidity, but now the coefficients C_V and Q_ν in Eqs. (29) and (30) include the temperature-dependent reduction factors. Note that the relevant parameter for the thermal evolution is $\tilde{T}$ rather

than T, such that the reduction factors are functions of $\tau(r) = \tilde{T}e^{-\Phi(r)}/T_c$, which is not constant throughout the star if we use a constant T_c. This radial dependence should be included in the integration of Eqs. (29) and (30). Since the τ dependence of the reduction factor is nonlinear, the variables $\tilde{T}$ and r cannot be separated, which means that the numerical integration must be carried out at each instance to solve the differential equation, cf. Eq. (28). To circumvent this we introduce an additional approximation by taking $T_c e^{\Phi(r)}$ a constant, such that the reduced temperature τ is constant inside the star. This decouples τ and r in Eqs. (29) and (30), which means we do the radial integration only once. Then Eq. (28) is independent of the radial coordinate and the reduction effect is represented by several extra τ-dependent terms in the coefficients. As is well known, the critical temperature T_c is a function of the density, however, the dependence is often uncertain. Because of the discrepancies between the pairing models, it is even unclear whether T_c for each type of baryon increases or decreases with baryon density in the range of interest. In fact, setting $T_c = $ const throughout the star also implies some kind of density dependence because the baryon density changes with the radius. In other words, as an ansatz, $T_c e^{\Phi(r)} = $ const is as reasonable as $T_c = $ const, even though the former seems unnatural because of its dependence on the macroscopic stellar structure. We use the former ansatz first because of its simplicity. Later we make a comparison between these two ansätze. In any case, $e^{-\Phi(r)}$ only varies smoothly and monotonically around 2, for example, from about 2.2 at $r = 0$ to about 1.4 at $r = R$ for the maximum mass neutron star with the hadronic equation of state, so we expect the difference between these two ansätze will not be of several orders in magnitude.

In the numerical calculation with the first ansatz, we set $T_c e^{\Phi(r)} = \tilde{T}(0) = 10^9$ K such that the baryons are superfluid from the start. This implies we have $T_c \approx 2.2 \times 10^9$ K at the central density while $T_c \approx 1.4 \times 10^9$ K near the surface. If, however, $\tilde{T}(0)$ were to be set higher, the reduction factors would at first not take effect and the direct Urca process would thus quickly reduce $\tilde{T}$ down to T_c after which it would be suppressed due to the onset of superfluidity and the cooling slowed down. This process takes only several seconds. On the other hand, if $\tilde{T}(0)$ would have been slightly lower, for example, above $0.1T_c$, then in the beginning the superfluid suppression would not be very strong and the direct Urca process could still cool the star to low temperature, i.e., the highly superfluid regime, within one year. Since the isothermal assumption we used here is virtually a later stage behavior, given a reasonable T_c and the well-accepted range of $\tilde{T}(0)$ of neutron stars, the result we presented in this section depends little on the accurate values of the temperature. As before, we take the neutron star with the hadronic equation of state as the basic example, then we study the stars with the mixed and nuclear equation of state.
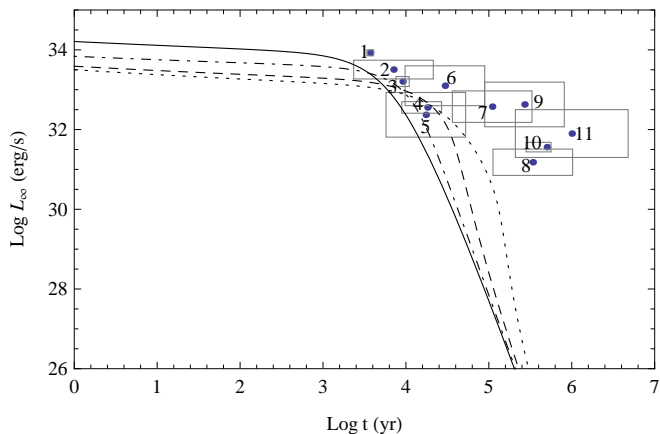
FIG. 20: The luminosity of a neutron star with the hadronic equation of state. The solid, dot-dashed, dashed, and dotted curves are for $\eta = 10^{-9}, 10^{-11}, 10^{-13}$, and 10^{-17}, respectively. The observational data are again shown for comparison.
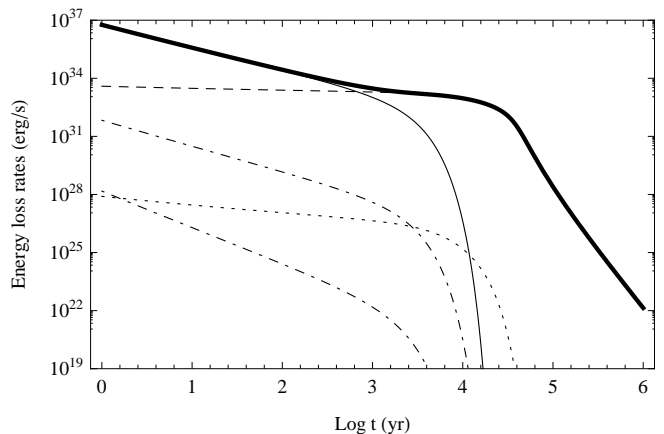

FIG. 21: The energy lost by the various processes in the neutron star with the hadronic equation of state, where the thick solid curve is the total energy loss rate, the thin solid curve is for the direct Urca process, the two dot-dashed curves are for the Cooper pair break-up processes with the upper one for the triplet-state pairing and the lower one for the singlet-state pairing, the dotted curve is for lepton bremsstrahlung, and the dashed curve is for photon radiation.
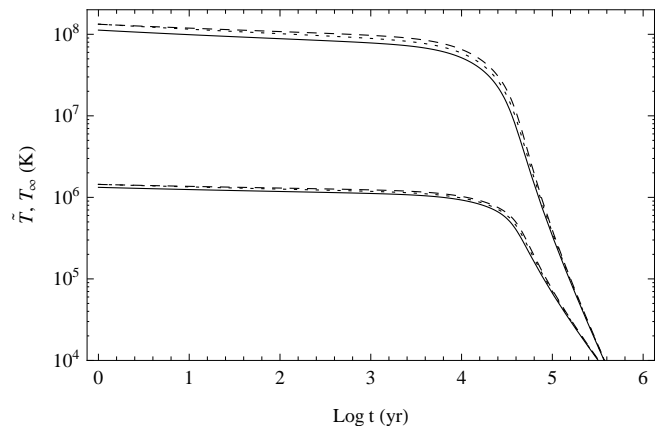

FIG. 22: The temperature evolution of the neutron star with the hadronic equation of state. The various curves represent different pairing types. The solid curves are for our standard setting, the dotted curves are when all baryons pair in the singlet-state, and the dashed curves are also for singlet-state pairing but with the reduction factor R_{AA} replaced by R_A^2. As before, the upper group is $\tilde{T}$ and the lower group is T_∞, respectively.

We find several general properties of the cooling behavior of stars containing superfluid matter from the numerical results. One obvious difference with the non-superfluid case is the shape of the cooling curve. Since the neutrino-emission processes, which dominate the early stage cooling, are strongly suppressed with decreasing temperature, the temperature stays high for a longer time and the shift to the photon radiation era takes place at higher temperatures. In contrast to the large slope in the non-superfluid case, we find a rather slowly decreasing plateau around $\tilde{T} \sim 10^8$ K and $T_\infty \sim 10^6$ K, followed by a much sharper turn to the photon radiation stage as can be seen in the following figures. Another difference can be seen in that the parameter η in the T_∞-T relation plays a more significant role. Because the neutrino-emission processes are suppressed due to superfluidity, photon radiation becomes more important at higher temperatures and the dependence on how the inner temperature is screened by the surface layer becomes more visible. We present the luminosity curves with different η in Fig. 20, where we see that the observational data favor moderate values of η. In the following, we usually use $\eta = 10^{-13}$.

Here some other general properties are summarized. First, we find that the heat capacity c_V of the baryons is quickly reduced as a consequence of superfluidity. Starting from $t \approx 1$ yr, the heat capacity is completely dominated by the lepton contribution, such that the pairing type of the baryons is seen to be of no importance to the heat capacity. Second, as was already shown in Fig. 19, neutrino emission via Cooper pair break-up is always negligible compared to the direct Urca process. We also find that the role of lepton bremsstrahlung in the cooling process is negligible since in the later stages when it dominates the neutrino emission, photon radiation has already become the dominant cooling effect. Therefore, the cooling process is determined only by the

direct Urca process and photon radiation. The various energy loss rates are shown in Fig. 21. Third, the direct Urca process depends on the type of pairing. However, this dependence is quite moderate. We show the different cooling curves for the various pairing types in Fig. 22. For singlet-state pairing, we see that neutrino emission is more strongly suppressed and the resulting temperature is slightly higher than the other types of pairing. This result confirms that the cooling behavior is not strongly dependent on the type of pairing of the baryons.

By comparing Fig. 20 and Fig. 17, we see that the luminosity curves in the superfluid case are much closer to observations than in the non-superfluid case. However, the curves do not agree with all the observational data except for the younger stars, namely number 1-5. This mismatch may lie in some important mechanisms which are neglected in the present calculation. For example, the magnetic field of the neutron star can affect the photon radiation at the surface [12] such that it no longer obeys the standard black-body radiation law and shift the photon-radiation era to a later time [35]. This reduction of photon radiation also decreases the luminosity, which is unfavorable according to the cooling curves shown in Fig. 20. However, there are some known heating mechanisms which are not considered here, for example, due to magnetic field energy and rotational energy (for more details, see Ref. [12] and references therein), such that the temperature and the luminosity can remain higher. Besides, note that sources such as number 10 and 11 may be old magnetars. As a consequence, the age estimates may not be correct, and the cooling history may be anomalous. Both are a result of the decay of the strong magnetic field: age estimates assume magnetic braking of rotation with a constant magnetic field, whereas the decay of the magnetic field results in heating of the neutron star [36]. We discuss these issues in future work.

Now we discuss the second ansatz, $T_c = $ const. Since $e^{-\Phi(r)} > 1$, if we set $T_c = \tilde{T}(0) = 10^9$ K we will have a lower T_c than in the previous ansatz and the baryons will not be superfluid everywhere inside the star at $t = 0$. To make a proper comparison between the two, we set $T_c = 1.9 \times 10^9$ K, where the extra factor 1.9 is the middle value of $e^{-\Phi(r)}$ inside the star (the outer value is taken at $r = 7$ km rather than at the surface since the direct Urca process starts around here, see Figs. 9 and 10). With this value of T_c, at $t = 0$, the baryons near the surface are superfluid while those in the core are not, since $\tau = \tilde{T} e^{-\Phi(r)}/T_c$ is bigger in the core. Nevertheless we expect the integrated results will be comparable to those of the previous ansatz. As a comparison, in Fig. 23, C_V and Q_ν are shown for these two ansätze. We see that the difference between the two increases with decreasing temperature and only becomes significant when their values are very small. Therefore, it is not surprising to find that their cooling curves are similar, as is shown in Fig. 24. The two curves are quite close except that the second ansatz has a little lower luminosity, because with $T_c = $ const the higher temperature in the core delays the suppression of the direct Urca process, such that the total cooling rate is larger in the beginning. Furthermore, the result of the ansatz $T_c = 10^9$ K mentioned above is also shown, where we can see that the high cooling rate due to the direct Urca process remains for a longer time and the luminosity is even more reduced after the neutron star has become completely superfluid. Here we see again that different initial conditions have little influence on the later-stage behavior.
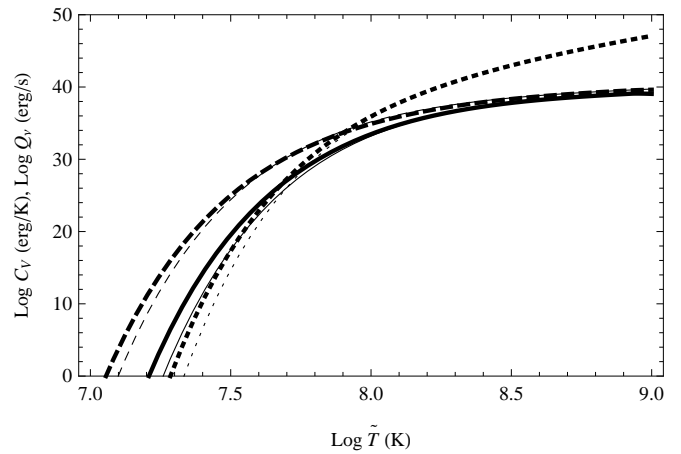

FIG. 23: The temperature dependence of C_V (solid curves for the singlet-state pairing contribution and dashed curves for the triplet-state pairing contribution) and Q_ν (dotted curves) calculated with the two different ansätze for T_c in the neutron star with the hadronic equation of state. For each quantity, the thick higher curve is for $T_c = $ const and the thin lower curve is for $T_c e^{\Phi(r)} = $ const, respectively.
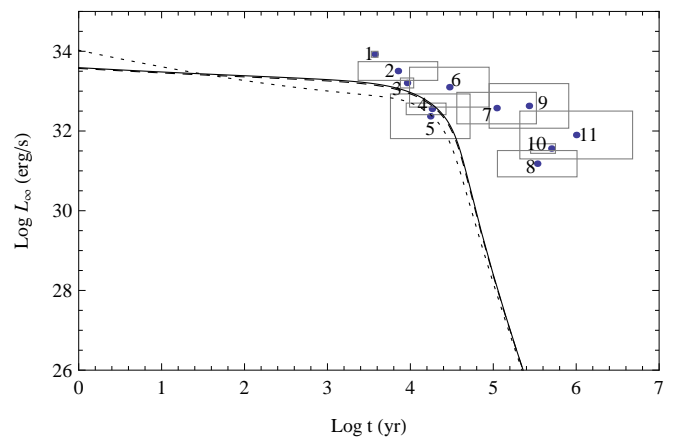

FIG. 24: The luminosity calculated with two different ansätze for T_c in the neutron star with the hadronic equation of state. The solid curve is for $T_c e^{\Phi(r)} = 10^9$ K and the dashed curve is for $T_c = 1.9 \times 10^9$ K, respectively. For comparison, the result with the ansatz $T_c = 10^9$ K is shown by the dotted curve. The observational data are again shown.

Finally, we briefly present the results for the neutron stars with the mixed and nuclear equation of state. For the nuclear case, we always take the neutrons and protons to pair in the triplet channel. The general arguments still apply, i.e., we only need to consider the direct Urca process and the photon radiation as the dominant cooling mechanisms. Without too much difference, the simple ansatz $T_c e^{\Phi(r)} = $ const will be used. The cooling behavior is mainly determined by the heat capacity, the direct Urca neutrino emissivity, and the photon radiation. These three parameters are not quite different among the various equations of state, even including the
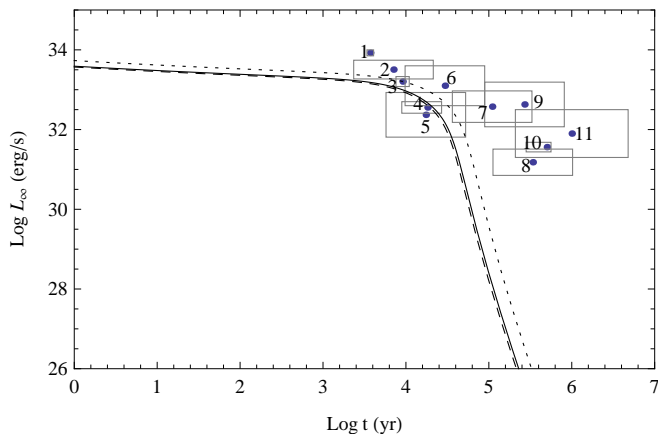
FIG. 25: The luminosity of the neutron stars with the various equations of state with the effect of superfluidity included. The solid, dashed, and dotted curves represent the hadronic, mixed, and nuclear equation of state, respectively. The observational data are again presented.

effect of superfluidity. The dominant contribution to the heat capacity is due to the leptons. The direct Urca process is dominated by the triplet-state paired baryons which make up the majority of the star and are less affected by superfluidity. The photon radiation is again just black-body radiation. Therefore, we expect that the cooling process should be similar in these three cases, whose luminosity curves are shown in Fig. 25. Compared to Fig. 17, besides the overall increase in the luminosity as previously discussed, there is some difference in the order of magnitude of the luminosity among these three equations of state. With superfluidity, the nuclear case always has the largest luminosity, which is due to the higher lepton fraction in the star. We find that the heat capacity of the leptons in the neutron star with the nuclear equation of state is about twice as large as that for the star with the hadronic or mixed equation of state. This larger lepton heat capacity becomes significant when the baryons (and the quarks) are highly superfluid. As can be seen in Eq. (28), the larger the heat capacity is, the higher the corresponding temperature should be. This explains the largest luminosity of the nuclear case in Fig. 25. Another difference is that, with superfluidity, the luminosity of the mixed case is always smaller than that of the hadronic case, while for the non-superfluid case as in Fig. 17, there is no such clear order. The reason also lies in the effect of superfluidity on the heat capacity, since in the mixed case the quark contribution is strongly suppressed due to superfluidity and completely neglected during our calculation. Of course, the neutrino emissivity from quarks is also reduced, but the reduction in the heat capacity is relatively stronger. This is because, without superfluidity, quarks contribute less to the neutrino emissivity than baryons, but their contribution to the heat capacity is comparable.

V. CONCLUSION AND DISCUSSION

We have carefully compared the thermal evolution of different types of neutron stars, namely with the

hadronic, the mixed phase of hadronic and strange quark matter, and the nuclear equation of state. We find that the direct Urca process is open in all of these cases and thus results in relatively fast cooling behavior. Although the details concerning the heat capacity and neutrino emissivity can be rather different in these cases, the cooling curves are quite similar after the stars become isothermal. However, the behavior in the early stages before the stars become isothermal could be significantly different, but such a study requires the knowledge of the thermal conductivity of these complex systems. The geometrical structure of the mixed phase is also expected to play an important role, although no decisive conclusion has yet been drawn.

As we have seen, the fast cooling in the non-superfluid case did not agree with observations. In order to remedy this discrepancy, superfluidity was introduced, which significantly reduces the efficiency of the direct Urca process as well as the heat capacity. The resulting cooling curve is much closer to the observational data. We also found that the particular pairing type of the superfluid baryons is not very important to the thermal evolution of the star. The thermal evolution after the star becomes isothermal is not strongly dependent on the initial temperature of the star or on the critical temperature related to superfluidity, as long as they are within reasonable ranges. The robustness of the results with superfluidity is quite helpful in order to remove the uncertainties concerning baryon superfluidity at high density. Note that the cooling process is almost completely determined by the direct Urca process and photon radiation even after including the effects due to superfluidity. The cooling curves of the neutron stars with the three equations of state are still quite similar when superfluidity is included. We expect that a calculation including the magnetic field and rotation gives an even better agreement with the observational data. Besides, since our nuclear model is geared originally towards nuclear matter near the saturation point, a further improvement of it may play an important role in getting a better agreement with the observations. By incorporating the properties at higher densities, e.g., the coupling constants for hyperons, it is possible to get cooling curves covering most of the observational data, as in Ref. [12].

[1] N. K. Glendenning, Astrophys. J. **293**, 470 (1985).

[2] N. K. Glendenning, Phys. Rev. D **46**, 1274 (1992).

[3] D. G. Yakovlev, A. D. Kaminker, O. Y. Gnedin, and P. Haensel, Phys. Rep. **354**, 1 (2001).

[4] J. M. Lattimer, C. J. Pethick, M. Prakash, and P. Haensel, Phys. Rev. Lett. **66**, 2701 (1991).

[5] C. Schaab, F. Weber, M. K. Weigel, and N. K. Glendenning, Nucl. Phys. **A605**, 531 (1996).

[6] D. Page and V. V. Usov, Phys. Rev. Lett. **89**, 131101 (2002).

[7] P. Freire, arXiv:0907.3219.

[8] P. B. Demorest *et al.*, Nature **467**, 1081 (2010).

[9] D. N. Voskresensky, M. Yasuhira, and T. Tatsumi, Phys. Lett. **B541**, 93 (2002); Nucl. Phys. **A723**, 291 (2003).

[10] F. X. Timmes, S. E. Woosley, and T. Weaver, Astrophys. J. **457**, 834 (1996).

[11] S. B. Popov, M. Colpi, M. E. Prokhorov, A. Treves, and R. Turolla, Astron. Astrophys. **406**, 111 (2003).

[12] D. Page, U. Geppert, and F. Weber, Nucl. Phys. **A777**, 497 (2006).

[13] T. Endo, Phys. Rev. C **83**, 068801 (2011).

[14] A. Ohnishi, D. Jido, T. Sekihara, and K. Tsubakihara, Phys. Rev. C **80**, 038202 (2009) and references therein.

[15] G. E. Brown, C.-H. Lee, and M. Rho, Phys. Rep. **462**, 1 (2008) and references therein.

[16] A. Y. Potekhin, arXiv:1102.5735.

[17] S. Weinberg, *Gravitation and cosmology*, John Wiley & Sons, New York (1972).

[18] J. Zimanyi and S. A. Moszkowski, Phys. Rev. C **42**, 416 (1990).

[19] B. D. Serot and J. D. Walecka, Adv. Nucl. Phys. **16**, 1 (1986).

[20] K. Nakamura *et al.* (Particle Data Group), Jour. Phys. G **37**, 075021 (2010).

[21] K. S. Thorne, Astrophys. J. **212**, 825 (1977).

[22] A. Y. Potekhin, G. Chabrier, and D. G. Yakovlev, Astron. Astrophys. **323**, 415 (1997).

[23] M. Prakash, M. Prakash, J. M. Lattimer, and C. J. Pethick, Astrophys. J. **390**, L77 (1992).

[24] N. Iwamoto, Ann. Phys. **141**, 1 (1982).

[25] C. O. Heinke and W. C. G. Ho, Astrophys, J. Lett. **719**, L167 (2010).

[26] D. Page, J. M. Lattimer, M. Prakash, and A. W. Steiner, Astrophys. J. Suppl. Ser. **155**, 623 (2004).

[27] D. G. Yakovlev, K. P. Levenfish, and Yu. A. Shibanov, Uspekhi Fiz. Nauk **169**, 825 (1999) (English trans. Physics-Uspekhi **42**, 737 (1999)).

[28] S. Balberg and N. Barnea, Phys. Rev. C **57**, 409 (1998).

[29] C. Schaab, S. Balberg, and J. Schaffner-Bielich, Astrophys. J. Lett. **504**, L99 (1998).

[30] K. P. Levenfish and D. G. Yakovlev D G, *Strongly Coupled Plasma Physics*, p.167, Eds. H. M. van Horn and S. Ichimaru, Rochester: Univ. of Rochester Press, (1993); Astron. Lett. **20**, 43 (1994).

[31] D. G. Yakovlev, A. D. Kaminker, and K. P. Levenfish, Astron. Astrophys. **343**, 650 (1999).

[32] L. B. Okun, *Leptons and Quarks*, North-Holland, Amsterdam (1984).

[33] A. D. Kaminker and P. Haensel, Acta Physica Polonica **30**, 1125 (1999).

[34] O. Y. Gnedin and D. G. Yakovlev, Nucl. Phys. **A582**, 697 (1995).

[35] D. Page and A. Sarmiento, Astrophys. J. **473**, 1067 (1996).

[36] J. S. Heyl and S. R. Kulkarni, Astrophys. J. **506**, L61 (1998).